NASA CONTRACTOR REPORT

NASA CR-261

NASA CR-261

ANALYTICAL AND EXPERIMENTAL INVESTIGATION OF PRESSURIZED TOROIDAL SHELLS

by P. F. Jordan

Prepared under Contract No. NASw-913 *by*
THE MARTIN COMPANY
Baltimore, Md.
for

NATIONAL AERONAUTICS AND SPACE ADMINISTRATION • WASHINGTON, D. C. • JULY 1965

NASA CR-261

ANALYTICAL AND EXPERIMENTAL INVESTIGATION OF PRESSURIZED TOROIDAL SHELLS

By P. F. Jordan

Prepared under Contract No. NASw-913 by
THE MARTIN COMPANY
Baltimore, Md.

for

NATIONAL AERONAUTICS AND SPACE ADMINISTRATION

For sale by the Clearinghouse for Federal Scientific and Technical Information
Springfield, Virginia 22151 – Price $3.00

FOREWORD

This final report, prepared by the Research Department of the Martin Company's Baltimore Division, summarizes the work done under National Aeronautics and Space Administration Contract No. NASw-913, Langley Research Center, Virginia. Also supported by this contract were two earlier publications, Refs. 1 and 7 of this report, and a paper "On the Pressurized Torus" (AIAA 65-146; no preprint) that was given by the Principal Investigator at the AIAA Second Aerospace Science Meeting, New York, January 25-27, 1965.

The NASA Technical Representative was Dr. Robert W. Leonard. The Principal Investigator, Dr. Peter F. Jordan, was assisted in the analysis work by Mr. Philip E. Shelley, while Mr. Robert J. Edwards was in charge of the test program.

The contractor's report no. is Research Report No. RR-64.

ABSTRACT

The behavior of a thin shell of revolution with a crown (example: torus) rather than a pole (example: sphere) is decisively determined by the shell mechanism at the crown. This fact permits an asymptotic analysis, which is so formulated that the solving functions become almost invariant with respect to the transition from the shell without internal pressure to the pressurized membrane. The transition range is discussed, in particular the transition to the membrane limit. Relations to previous formulations are given. Tests in which a 54-inch diameter torus shell was subjected to both pressurization and axial load led to excellent agreement, in general, with analytical predictions.

Author

CONTENTS

I. INTRODUCTION

The problem to be discussed in this paper is that of a thin-walled shell of revolution with a crown ("torus-type shell"); of particular interest is the effect of an internal pressure p on the behavior of this shell. The stresses and deformations that arise from pressurization alone are one subproblem; the reactions of a pressurized shell to an external load are the second. For the first, linear membrane theory, though it is inconsistent mechanically, yields a fair approximation to the direct stresses that determine the design; the problem is to determine the corrections that, if added to the result of linear shell theory, produce a consistent solution. For the second subproblem, linear membrane theory has no answer.

In Ref. 1, the problem was discussed, in terms of a quasi-linear shell theory, in a formulation that makes it apparent that there has to be a continuous transition between the two limit cases, the unpressurized shell which has only bending stiffness, and the pressurized membrane which has only pressure stiffness. In fact, there is a remarkable qualitative similarity between the two limit solutions. Indeed, the mathematical problem, though it is of second order in the membrane limit, of fourth order elsewhere, with a continuous shift in emphasis from the second order to the fourth order term between the two limits, is always a problem with a double transition point, and this determines the essential character of the solution.

The existence of a double transition point has the effect that the crown mechanism, the shell mechanism which occurs in a close neighborhood of the crown (i.e., the transition point) becomes the decisive mechanism which dominates the behavior of the shell. This, in turn, has the effect that an asymptotic formulation of the analysis, a formulation in which only the shell parameters at the crown itself do appear, becomes sufficiently accurate for most practical purposes in a large range of applications.

This fact can be stated in a precise form by means of the formal solution of the membrane problem that is given in Ref. 7 (it had been utilized earlier

by Clark[4] in an investigation of the unpressurized torus). Based on it, the axial stiffness of the torus shell was determined throughout the transition range of Ref. 1.

It was shown in Ref. 1 that the asymptotic solution is described by a pair of transcendental functions which, in the two limits, are equivalent with functions defined by Clark [4] and by Sanders and Liepins[3]. An evaluation, more accurate than the approximation given in Ref. 1, of the transition itself was given by Rossettos and Sanders[5]. However, the relations between the various presentations were not clear. In Chapter II of this paper, a formulation is developed which makes the solving functions almost invariant with respect to the transition; the relations between the various presentations are established, and the transitions to the two limits are discussed in detail. In particular, an asymptotic presentation of the transition to the membrane limit is given.

In Chapter III, the results of the asymptotic analysis are compared with experimental results, and are shown to be adequate for their purpose. More refined methods of analysis are discussed in Chapter IV.

Appendix A describes a computer program that has been developed, and has been used to check and improve the reliability of published tabulations[4,5,6]; this program can be used to solve the problem in its more general formulation, without recourse to the asymptotic simplification. Appendix B describes the details of the test program. Appendix C, a brief discussion of a paper by A. Kalnins[9], to be published, is concerned with a point that has sometimes led to conceptual difficulties.

II. ASYMPTOTIC SOLUTION OF THE SHELL EQUATION

1. Asymptotic Formulation

The fourth order differential equation which describes the problem of the thin-walled, pressurized torus-type shell, loaded axially, reads in its simplified (asymptotic) form [compare Ref. 1, Eq. (40)]

$$fx^2 - Ak^4 f'' + Bk^6 \bar{f}^{IV} = \epsilon_0 k^2 \tilde{p}(x) + x_0 kx \tag{1}$$

This equation, which forms the basis of our discussion, is briefly described next. The unknown function $f \equiv f(x)$ which is closely related to the meridional shell rotation β

$$\beta \cos \phi_0 = f(r-a) - x_0 \tag{2}$$

describes all stresses and deformations of the shell; thus the solution of Eq. (1) is equivalent to the solution of the shell problem.

Some of the notation is indicated in Fig. 1 where rR is the axis distance of a shell point, R the meridional radius, a the opening ratio, ϕ_0 the meridional tangent angle of the undeformed shell. Thus (r-a) is the nondimensional horizontal distance from the crown point r = a ($\phi_0 = 0$) of the undeformed shell. Equation (1) as such is not confined to the circular torus with uniform wall thickness h and uniform internal pressure p; R, h and p may vary (slowly) along the shell meridian. In this general case (which is not discussed here in detail; reference is made to Ref. 1) R, h and p are always understood, in the present formulae, to be the respective values at the crown r = a.

The independent variable x of Eq. (1) is derived from the coordinate (r-a) by means of the stretching transformation

$$x = k(r-a) \tag{3}$$

(= k sin ϕ_0 in the case of a circular torus)

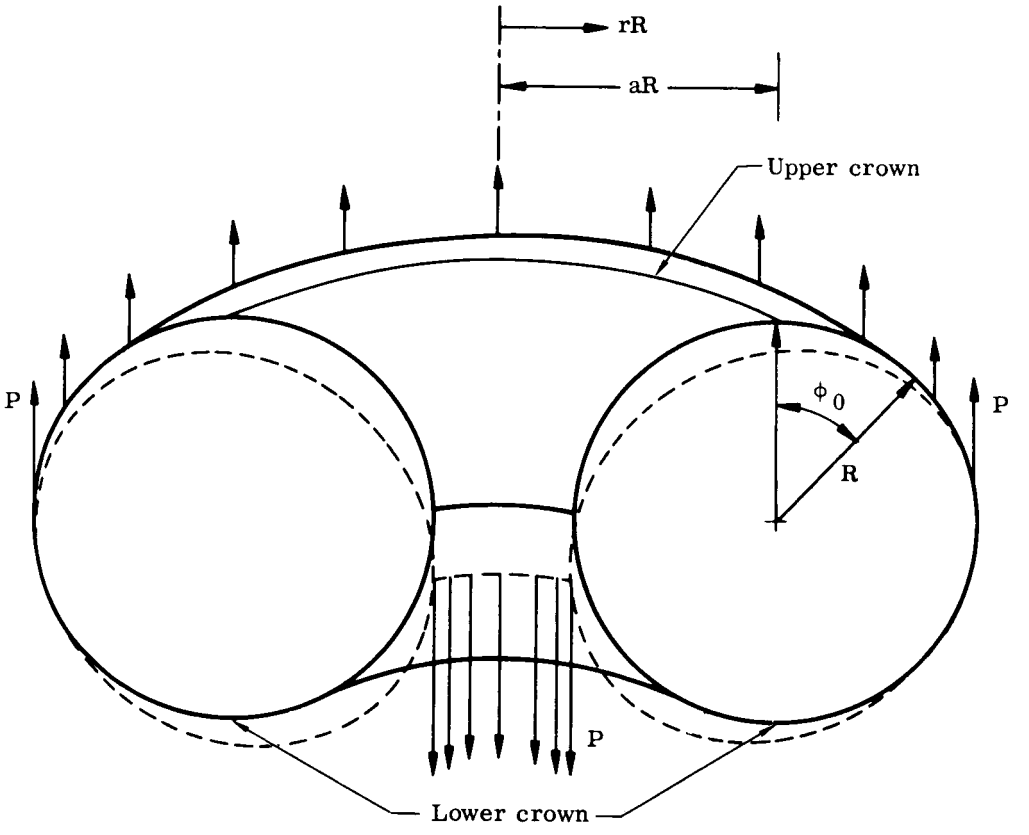

Fig. 1. Circular Torus Shell Under Axial Load P

where k is a constant, so far arbitrary. The second order differential term represents the pressure stiffness, the fourth order term the bending stiffness of the shell; we have

$$Ak^4 f'' \equiv \epsilon_0 a^2 k^4 \frac{d^2 f}{dx^2} \quad ; \quad \epsilon_0 \equiv \frac{pR}{Eh}$$

$$Bk^6 \bar{f}^{IV} \equiv \frac{(ha/R)^2}{12(1-\nu^2)} k^6 \cdot \left\{ \left(\frac{1}{x} (xf)'' \right)'' - \frac{4}{x^3} f'_x = 0 \right\} \tag{4}$$

It is desirable to choose k such that the sum of the two products

$$\bar{A} \equiv Ak^4 \quad ; \quad \bar{B} \equiv Bk^6 \tag{5}$$

is of order 0(1). In this case the length 2R/k becomes a measure of the effective width of the crown range, the range where the crown mechanism, which dominates the behavior of a shell with an unrestrained crown and which is the subject of the present investigation, takes place. If the thickness ratio h/R and the reference strain ϵ_0 (a mean value of the strain produced by pressure) are both small enough to justify the use of quasilinear theory, and if furthermore the opening ratio a is not very large (this we also assume henceforth) then k will be a fairly large number.

The two stiffness terms, Eq. (4), are asymptotic simplifications. To be more exact, we would have to replace f'' by

$$f'' \rightarrow \left[\left(1 + \frac{d}{k} x \right) f'' + \frac{e}{k} f' + 0\left(\frac{1}{k^2} \right) \right] \tag{6}$$

and would have a correspondingly refined expression for $\bar{f}^{IV}$, with constants d, e $\cdots$ of order 1/a. These constants would also contain coefficients of series describing R, h and p if these quantities would vary along the shell meridian. However, as k is fairly large, the solution of the asymptotically simplified equation Eq.(1) will describe the overall behavior of the shell with an accuracy that is sufficient for most practical application. This statement will be seen to be confirmed by our experimental results.

The first term on the right hand side of Eq.(1) arises from the pressure load on the undeformed shell. In the case that R, h and p are constants, we have

$$\tilde{p}(x) = \frac{a}{2r} \cos^2 \phi_0 \tag{7}$$

A modified expression arises if these quantities vary along the meridian. The second term allows for a crown shift, that is, a deformation of the shell meridian such that its crown $\phi = \phi_0 + \beta = 0$ is shifted inward, with respect to the original crown point $\phi_0 = 0$, by the distance $x_0 R$.

2. Normalized Solutions T_n

In discussing the solution f of Eq.(1) we confine our present attention to those solutions for which the differential terms in Eq.(1) disappear away from the crown, such that, as |x| increases,

$$fx^2 \to \epsilon_0 k^2 \tilde{p} + x_0 kx \tag{8}$$

This limit for f represents a result of linear membrane theory; it has a singularity, and is hence meaningless mechanically, for $x \to 0$, but the mechanically correct solution coverges toward it as |x| increases to 0(1), and becomes practically undistinguishable from it for $|x| > 4$, say, supposing that the boundaries of the shell are sufficiently far away from the crown.

Suppose that, for a given set $(\bar{A}, \bar{B})$ of parameter values, Eq.(5), we have obtained the two solutions, T_0 and T_1, of the equation

$$T_n x^2 - \bar{A} T_n'' + \bar{B} \bar{T}_n^{IV} = x^n \qquad (n = 0, 1)$$

$$T_n \to x^{n-2} \quad \text{for} \quad |x| \to \infty \tag{9}$$

Then, if we further write

$$\tilde{p}(x) = c_0 - c_1 \left(\frac{x}{k}\right) - \tilde{\tilde{p}}(x) \left(\frac{x}{k}\right)^2$$

$$\left(= \frac{1}{2} - \frac{1}{2a} \left(\frac{x}{k}\right) - \frac{a^2-1}{2ar} \left(\frac{x}{k}\right)^2 \text{ for the uniform circular torus}\right)$$

we have

$$f = \epsilon_0 \left(k^2 c_0 T_0 - k c_1 T_1 - \tilde{\tilde{p}}(x)\right) + x_0 k T_1 \tag{10}$$

within the accuracy of the asymptotic analysis.

The task that remains is to prepare a tabulation of a suitable set of basic solutions T_n. The first problem that arises in this respect is how best to choose k, and thus the set of parameters $(\bar{A}, \bar{B})$ for T_n, for any given set of mechanical parameters (A, B). One will, of course, choose k such that $(\bar{A}, \bar{B})$ becomes a one-parametric set.

As an example, we might choose k such that the resulting set $(\bar{A}, \bar{B}) \equiv (\bar{A}^*, \bar{B}^*)$ fulfills the condition

$$\bar{A}^* + \bar{B}^* = 1 \tag{11}$$

The set of solutions T_n that belongs to this set $(\bar{A}^*, \bar{B}^*)$ we denote by T_n^* There are two limit cases: $(\bar{A}^*, \bar{B}^*) = (0, 1)$, the case of zero internal pressure p, and $(\bar{A}^*, \bar{B}^*) = (1, 0)$, the case of a membrane shell without bending stiffness. The intermediate range, $0 < \bar{A}^* < 1$, may be called the transition range, and $\bar{A}^*$ may be considered as the single transition parameter that describes the nature of the given mechanical problem.

The two limit sets T_n^* have been discussed in Ref. 1 (where they are denoted by S_n and T_n respectively). They are shown in Fig. 2, where their x-coordinate is denoted by x^*, together with the functions, $1/x^{*2}$ for $n = 0$, $1/x^*$ for $n = 1$, toward which they converge as $|x^*| \to \infty$.

Inspection of Fig. 2 reveals that there is a qualitative similarity between the two sets of limit solutions T_n^*, and suggests that there should be a continuous transition between the two limits as the transition parameter $\overline{A}^*$ is increased from zero to one. It further suggests that the similarity of the two limit sets might be enhanced considerably if k, and thus $(\overline{A}, \overline{B})$, would be defined not by Eq.(11) but by the condition

$$(T_{0\, x = 0} \equiv)\ T_0\ (0) = 1 \tag{12}$$

which normalizes the amplitude of the function T_0.

The two normalized limit sets T_n are shown in Fig. 3. Their close similarity is indeed striking; it is particularly interesting that this applies not only to the functions T_0, where, to a degree, it is a direct consequence of Eq.(12), but it applies simultaneously to the functions T_1. Implied by this similarity is of course a corresponding similarity, in their mechanical contributions to the crown mechanism, of the two types of shell stiffness, bending stiffness and pressure stiffness.†

It further turns out (see below) that the transition between the two limit sets T_n is quite smooth, almost linear, if it is plotted over a suitable transition parameter. The normalized set T_n is thus a particularly convenient basis for practical analyses as well as for comparing the crown mechanisms in different parts of the transition range; in consequence, it is used as such a basis in our subsequent discussions. In what follows, T_n, $\overline{A}$ and $\overline{B}$ always refer to the normalized quantities.

---

†Compare, for instance, the similarity of the two limits of the normalized deformation curve, Fig. 5 of Ref. 1.

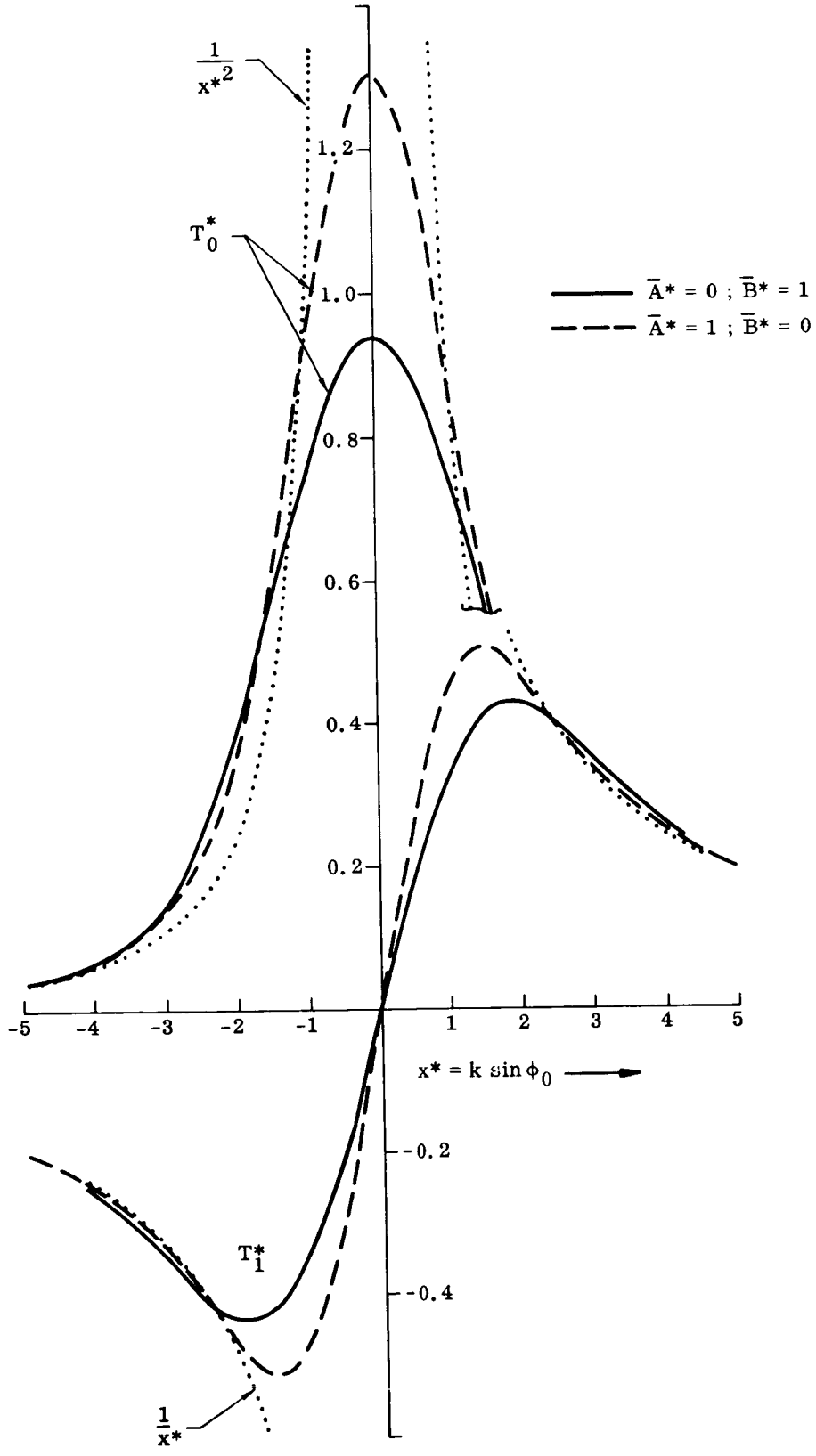

Fig. 2. Basic Solutions T_n^*

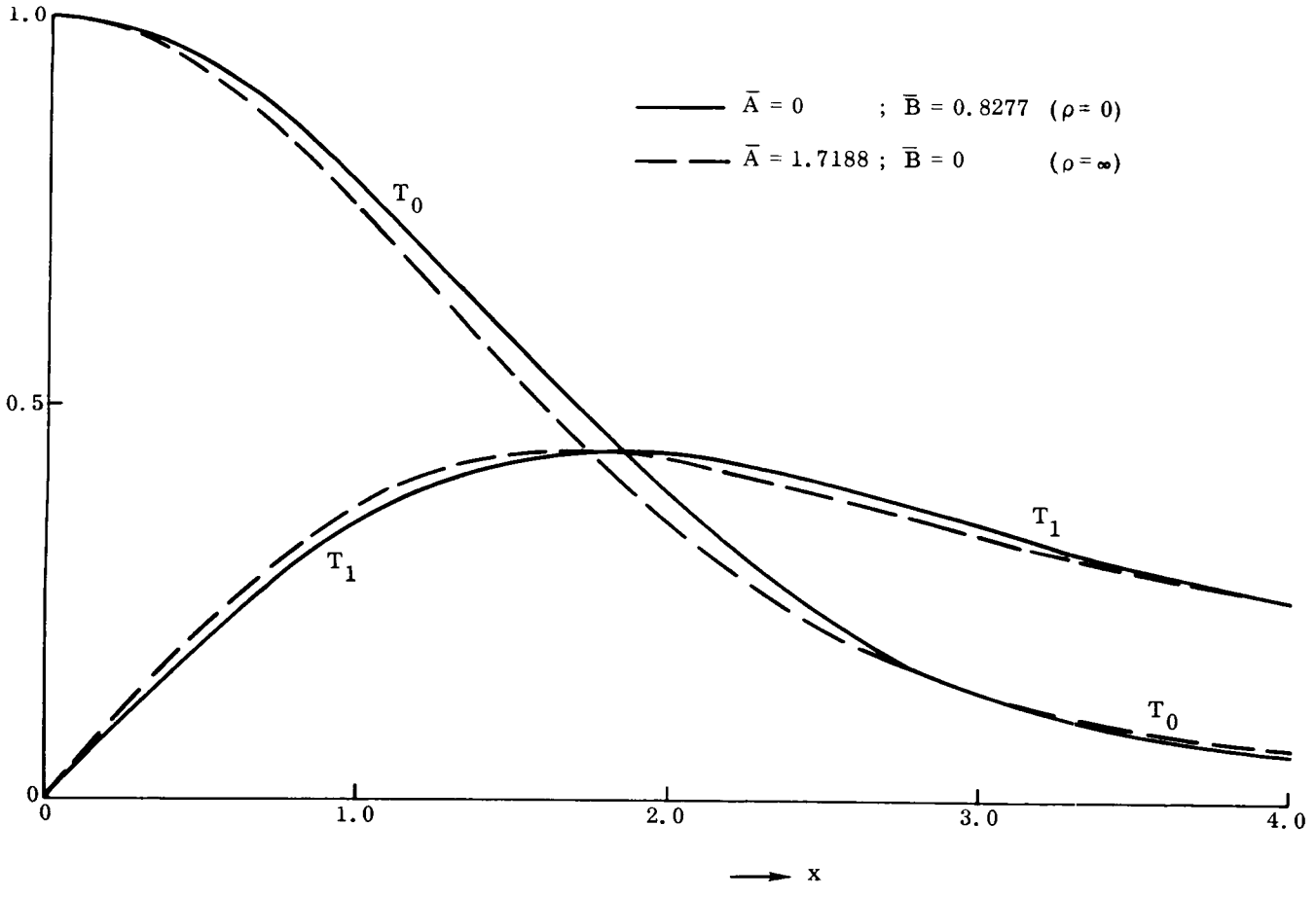

Fig. 3. Normalized Basic Solutions T_n

The relation between $\bar{A}$ and $\bar{B}$ does not follow directly from Eq.(12), and it appears necessary to calculate T_n in two steps. Suppose that Eq.(9) has been solved for a given pair $(\bar{A}^*, \bar{B}^*)$ [not necessarily one that obeys Eq.(11)]. Denote the corresponding x-coordinate by x^*, and define $T_n^{*''} \equiv d^2 T_n^*/dx^{*2}$, etc. Thus

$$T_n^* x^{*2} - \bar{A}^* T_n^{*''} + \bar{B}^* \bar{T}_n^{*iv} = x^{*n} \tag{13}$$

Set $\kappa^2 = T_0^*(0)$ and apply the transformation

$$\kappa x^* \equiv x \quad ; \quad \kappa^n T_n^* = \kappa^2 T_n \tag{14}$$

Then

$$T_n x^2 - \bar{A}^* \kappa^4 T_n'' + \bar{B}^* \kappa^6 \bar{T}_n^{iv} = x^n \tag{15}$$

and $T_0(0) = 1$. It follows that the T_n are the required normalized solutions, and that $\bar{A} = \bar{A}^* \kappa^4$, $\bar{B} = \bar{B}^* \kappa^6$.

As the limit functions T_n^*, Fig. 2, are well known, the limit functions T_n, Fig. 3, are readily determined by means of Eq. (14). Some significant numerical values are listed in the table that follows:

$\bar{A}$	$\bar{B}$	$-T_0''(0)$	$T_1'(0)$	c
0	$(-1/3)!^3/3$ ≈ 0.8277	$\frac{(1/3)!}{(-1/3)!^2}$ ≈ 0.4870	$[2(1/3)!(-1/3)!]^{-1}$ ≈ 0.4135	$\frac{\pi\sqrt{(-1/3)!}}{2\sqrt{3}(1/3)!}$ ≈ 1.1818
$\left[\frac{(1/4)!}{(-1/4)!}\right]^2 \pi$ ≈ 1.7188	0	$1/\bar{A}$ ≈ 0.5818	$\pi/4\bar{A}$ ≈ 0.4570	$(-1/4)!^2 \bar{A}^{1/4}/\sqrt{2}$ ≈ 1.2158

(16)

Among the numbers listed, the constant

$$c \equiv \int_0^\infty (1 - x T_1)\, dx \tag{17}$$

determines the stiffness of the complete circular torus under axial load.

Significant properties of the functions T_n have been investigated throughout the transition range, partly on the basis of available tabulations, partly by means of computer programs that were prepared for this purpose. The results will be presented later; first, the relations to the existing tabulations will be discussed.

From inspecting either Eq. (9) or Fig. 3, one would expect that the complete transition, from one limit to the other and including both limits, should not involve any specific difficulties. On the other hand, the relations between the available tabulations are not immediately obvious. The membrane limit ($\overline{B} = 0$), first discussed by Jordan[2], was brought into an asymptotic form by Sanders and Liepins[3]. The zero pressure limit ($\overline{A} = 0$) was discussed in particular by Clark[4]. The approaches used to formulate these theories differed in the two limit cases; the present joint formulation, developed in Ref. 1, is a generalization of Ref. 2, to which the tabulations of Ref. 3 are fairly directly related, but incorporation into Ref. 1 of the functions tabulated in Ref. 4 required a transformation the significance of which was not discussed in Ref. 1.

For the analysis of the transition range proper, an approximate procedure was used in Ref. 1. This procedure, while it did not involve any difficulties near the limits, did however involve a piecing together of two branch solutions in the center of the transition range. Rossettos and Sanders[5], on the other hand, in discussing the transition range, used a formulation which, while it is continuous throughout this range, deteoriates as either limit is approached.

In Ref. 5, tables are given which (include the limit $\overline{A} = 0$ but not the limit $\overline{B} = 0$) are the only tabulations available for the transition range. In the next two sections, relations between Ref. 5 and the present presentation will be established, and the transition will be discussed. In the subsequent sections, the behavior at the limits will be investigated.

3. Relations to the Formulation of Rossettos and Sanders

In order to split the fourth order differential equation Eq. (9), with $\overline{T}^{IV}$ defined according to Eq. (4), into a system of two second order differential equations, introduce new functions f_n by

$$xT_0 = f_0 \;;\; xT_1 = (1 + C)f_1 - C$$

$$\text{where } C = 2\bar{B}\, T_1'(0)/\bar{A} \tag{18}$$

with the alternative form

$$xT_1 = \frac{f_1 - f_1(0)}{1 - f_1(0)} \tag{18a}$$

With this, and by introducing auxiliary functions g_n, Eq. (9) becomes

$$-\bar{A} f_n + \bar{B} f_n'' - x g_n = 0$$

$$g_n'' + x f_n = x^n \tag{19}$$

This system closely resembles the systems Eqs. (56) and (57) in Ref. 5 which define tabulated functions f_A, f_B, g_A and g_B and which read, if we use $\bar{x}$ here as the coordinate for these functions and read f_A'' as $d^2 f_A/d\bar{x}^2$, etc.,

$$-\rho f_A + f_A'' - \bar{x} g_A = 0$$

$$g_A'' + \bar{x} f_A = 1 \tag{20}$$

$$-\rho f_B + f_B'' - \bar{x} g_B = 0$$

$$g_B'' + \bar{x} f_B = -\bar{x} \qquad (21)$$

That is, in Ref.5 k is chosen such that $Bk^6 = 1$. This defines a transition parameter ρ:

$$\rho = Ak^4 = \frac{A}{B^{2/3}} \equiv \frac{\bar{A}}{\bar{B}^{2/3}} \equiv \frac{\bar{A}^*}{\bar{B}^{*2/3}} \qquad (22)$$

The transformations that relate Eqs. (19), (20) and (21) resemble the transformation Eq. (14):

$$f_0 = \kappa f_A \quad ; \quad \kappa^2 g_0 = g_A \quad ; \quad \bar{x} = \kappa x$$

$$f_1 = -f_B \quad ; \quad \kappa^3 g_1 = -g_B \quad ; \quad \bar{A}\kappa^4 = \rho \qquad (23)$$

The normalization condition Eq. (12) requires

$$T_0(0) = f_0'(0) = \kappa^2 f_A'(0) = 1 \qquad (23a)$$

This determines κ, and leads to the following expressions for the quantities listed in (16):

$$\bar{A} = \rho \left[f_A'(0)\right]^2 \quad ; \quad \bar{B} = \left[f_A'(0)\right]^3$$

$$T_0''(0) = \frac{1}{3f_A'(0)} \left[\rho + \frac{g_A(0)}{f_A'(0)}\right] \quad ; \quad T_1'(0) = \frac{-\rho}{2f_A'(0)} \cdot \frac{f_B(0)}{1 + f_B(0)}$$

$$c = \frac{\sqrt{f_A'(0)}}{1 + f_B(0)} I_1(\infty) \qquad (24)$$

4. Interpolations Through the Transition Range

The formulation of Ref. 5, and hence the relations in Eq. (24), involve certain difficulties as $\rho \to 0$ (zero pressure limit) or $\rho \to \infty$ (membrane limit). The solution of Eq. (21) for $\rho \to 0$ is $f_B = -1$; $g_B = 0$; correspondingly, $C \to \infty$ in Eq. (18), and T_1 thus becomes undetermined. In the limit $\rho \to \infty$ Eqs. (20), (21) become useless. Indeed, large values of ρ contradict a requirement that was spelled out in connection with Eq. (5). A consequence is that, in terms of the coordinate $\bar{x}$, the crown range increases† indefinitely as $\rho \to \infty$.

On the other hand, if $\bar{A}$, $\bar{B} \cdots$, calculated by means of Eq. (24) from the numerical values of Ref. 5, are plotted over $\bar{A}$ together with their exactly known limit values (16), a continuous and almost linear behavior is found that includes both limits. However, $\bar{A}$ is not a practical transition parameter for several reasons; $\bar{A}$ cannot, in general, be calculated directly from the given mechanical parameters, A and B, and $\bar{A}$ is a transcendental number at the membrane limit. A practical transition parameter is

$$\begin{aligned} \rho^* &= (1 + 4\rho^{-3/2})^{-2/3} = \frac{A}{(A^{3/2} + 4B)^{2/3}} \\ &\to \frac{\rho}{4^{2/3}} \text{ for } \rho \to 0 \\ &\to 1 - \frac{8}{3\rho^{3/2}} \text{ for } \rho \to \infty \end{aligned} \tag{25}$$

Thus $\rho^* = 0$ designates the zero pressure limit, $\rho^* = 1$ the membrane limit. Plotted over ρ^*, Fig. 4, both $\bar{A}$ and $\bar{B}$ describe smooth curves with little curvature. (A fairly large gap, for which no intermediate values are available, exists between $\rho = 1$ and $\rho = 5$).

†By "crown range" is meant that range around $x = 0$ where the functions T_n differ appreciably from the functions $1/x^2$ and $1/x$ respectively toward which they converge as $|x|$ increases. Figure 3 shows that, in terms of the coordinate x, this crown range is practically invariant with respect to the transition parameter.

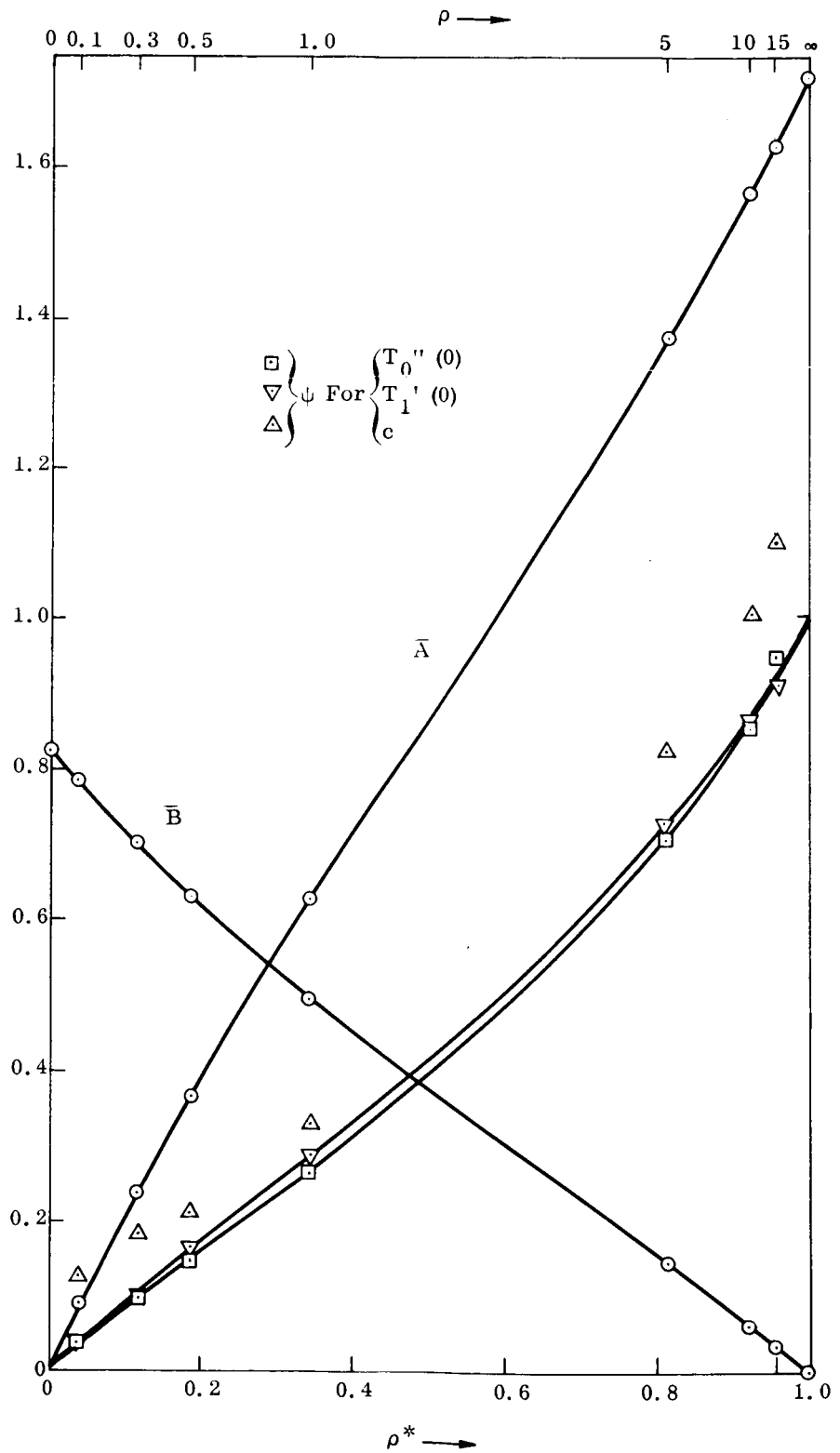

Fig. 4. The Transition Range

The quantities $-T_0''(0)$, $T_1'(0)$ and c, which vary relatively little between the two limits, are shown in Fig. 4 by means of interpolation functions ψ, formed in all three cases as is shown here for c

$$c = c_{\rho*=0} + (c_{\rho*=1} - c_{\rho*=0})\,\psi \tag{26}$$

In viewing the points for ψ in Fig. 4, one has to realize that not only are the differences which ψ interpolates relatively small but that, furthermore, application of Eq. (24) involves itself the formation of small differences of large numbers in some cases. This applies in particular to the integral c; here, even though the respective tables of Ref. 5 give 4 or 3 significant digits, the points for ψ are badly defined and their apparent scatter simply indicates this uncertainty.

Another fact that has to be taken into consideration is that the tables of Ref. 5 are not always exact to the last digit given. An example: From Eqs. (16) and (24)

$$f'_{A\,\rho=0}(0) = (-1/3)!/\sqrt[3]{3} = 0.9388929\ldots$$

while Ref. 5 gives 0.9386. This is not an isolated misprint; rather, the $f'_{A\ \rho=0}$ table of Ref. 5 deviates by about the same amount down to $\bar{x} = 1.0$ (as is readily established by comparison with the table for T_i' in Hetényi and Timms[6]). Prompted by this observation, we computed the numbers that determine $T_0''(0)$ and $T_1'(0)$ according to Eq. (24) for $\rho = 1$, 5, 10 and 15 by an accurate method (see Appendix A). The errors in Ref. 5 that we found remained constant in overall magnitude over the ρ-range, and were small enough so that their effect is not visible in Fig. 4, except for $\rho = 15$, where the ψ-points for $T_0''(0)$ and $T_1'(0)$ deviate from respective smooth curves that would include the point $\psi = 1$ for $\rho \to \infty$. (Indeed, the sensitivity of Eq. (24) increases as $\rho \to \infty$.) On the other hand, the ψ-points for $\rho = 15$ that we calculated from our accurate results lie on the curves that are drawn in Fig. 4. These curves we defined more precisely by determining their tangents at the limit $\rho \to \infty$. How this was achieved will be discussed below, following a discussion of the limit $\rho = 0$.

Summarizing Fig. 4: the three ψ-curves are fairly similar in nature but are not identical.

Figure 4 is characteristic of the nature of the transition. Corresponding ψ-curves can be drawn for any other quantity, e.g., for $T_n(x)$ for any given x. Where this was done (so far in an exploratory manner), a smooth behavior has always been found.

5. The Zero Pressure Limit

In the limit $\rho \to 0$, the presentation of Ref. 5 becomes undeterminate; e.g., the equations for stresses and rotation (Eqs. (73), (74), (76), l.c.) contain, in their more important terms, respectively

$$\frac{g_B}{\rho} \quad , \quad \frac{f_B + 1}{\rho} \to \frac{0}{0} \quad \text{as } \rho \to 0 \tag{27}$$

On the other hand, in the presentation of Clark[4], who investigated the case of zero pressure, the stresses are given essentially by a function T_i, and the rotation by a function T_r; comparison of the numerical tables in Refs. 4 and 5 shows that (apart from minor numerical discrepancies)

$$f_{A\,\rho=0} = T_i \quad ; \quad g_{A\,\rho=0} = T_r \tag{28}$$

That is, in Ref. 4, f_A, g_A seem to take the places of g_B, f_B.

This riddle is readily resolved. We show first that Eq. (28) is correct. Clark[4] uses a complex function

$$T \equiv T_r + i\,T_i$$

and defines

$$T'' - i\,\bar{x}\,T = 1 \qquad (T'' \to 0 \quad \text{for } \bar{x} \to 0) \tag{29}$$

Separating real and imaginary parts in Eq. (29) yields

$$T_i'' - \bar{x}\, T_r = 0$$

$$T_r'' + \bar{x}\, T_i = 1 \qquad (29a)$$

If we insert Eq. (28), this becomes identical with the limit $\rho \to 0$ of Eq. (20). It follows that Eq. (28) is correct.

In order to discuss the functions f_B and g_B, set

$$f_B = -\rho \tilde{f}_B - 1$$

$$g_B = \rho \tilde{g}_B$$

and insert into Eq. (21). Then

$$\tilde{g}_B'' - \bar{x}\, \tilde{f}_B = 0$$

$$\tilde{f}_B'' + \bar{x}\, \tilde{g}_B - \rho \tilde{f}_B = 1$$

Comparison with Eq. (20) shows that

$$\tilde{g}_B \to f_A \;; \qquad \tilde{f}_B \to g_A \qquad (\text{as } \rho \to 0)$$

so that in Eq. (27)

$$\frac{g_B}{\rho} \to T_i \;; \qquad \frac{f_B + 1}{\rho} \to T_r \quad (\text{as } \rho \to 0) \qquad (30)$$

By means of Eq. (30), the asymptotic limits of the result of Ref. 5 transform into those of Ref. 4 as $\rho \to 0$.

Equations (28) with (23), (18) and (14) also establish that for $\rho \to 0$ the two coordinates, $\bar{x}$ and x^*, become identical, and that

$$T_i = f_A = x^*\, T_0^* \qquad (\rho = 0) \qquad (31)$$

On the other hand, Eq. (18) becomes undeterminate for T_1 as $\rho \to 0$. In order to resolve this difficulty, eliminate first T_r, next T_i in Eq. (29a). Thus

$$\left(\frac{1}{\bar{x}} T_i''\right)'' + \bar{x} T_i = 1$$

$$\left(\frac{1}{\bar{x}} T_r''\right)'' + \bar{x} T_r = \frac{2}{\bar{x}^3}$$

Comparing these equations with Eqs. (9) and (4), setting $\bar{A} = 0$, $\bar{B} = 1$, we find that the first confirms again Eq. (31), while the second leads to

$$T_r = g_A = \frac{1}{2T_1^{*\prime}(0)} (x^* T_1^* - 1) \qquad (\rho = 0) \tag{32}$$

Equations (30), (31) and (32) are the complete relations, for the limit $\rho = 0$, between the three sets of basic functions.

A note on published numerical tabulations for $\rho = 0$: the tables by Clark[4] give 3 decimals with a number of rounding-off errors; in a few cases, the last digit deviates by two units. Five decimal tables have been published by Hetényi and Timms[6]; these tables are correct up to $\bar{x} = 2.6$ (disregarding a minor rounding-off error at $\bar{x} = 2.0$) but the tables for T_i and T_i' contain an oscillating error as $\bar{x}$ is increased further; the maximum error is ten units in the last digit. The reverse is true for the four decimal tables of Rossettos and Sanders[5]; as aforesaid; these tables are accurate for $\bar{x}$ large but the last digit is unreliable for $\bar{x} \to 0$.

6. The Membrane Limit

In the limit $\rho^* \to 1$ the factor $\bar{B} \to 0$, and the fourth order equation Eq. (9) reduce to a second order equation. Such a reduction is of some mathematical interest; one would like to be sure that the smooth interpolation that is suggested by Fig. 4 is indeed valid. That this is the case will be shown here by means of analysis that becomes exact asymptotically as $\rho^* \to 1$. In this analysis, use is made of a formalism that was developed in Ref. 7.

The functions that are denoted by T_0 and T_1 in Ref. 7 are identical respectively to the limits $\rho^* \to 1$ of the functions T_0^* and T_1^* as defined in this paper. In the present section we denote these limit functions by T_n^*.

Starting from Eqs. (19), we use the transformation

$$\bar{x} = \kappa x \;;\; \bar{g}_n = \kappa^{n+2} g_n \;;\; \bar{f}_n = \kappa^{n-1} f_n \;;\; \kappa^4 \bar{A} = 1$$

and obtain

$$\bar{f}_n - \delta \bar{f}_n'' + \bar{x}\, \bar{g}_n = 0$$

$$\bar{g}_n'' + \bar{x}\, \bar{f}_n = \bar{x}^n \;;\quad \delta \equiv \frac{\bar{B}}{\bar{A}^{3/2}} \equiv \rho^{-3/2} \tag{33}$$

Setting

$$\bar{f}_n \equiv \bar{x}\, T_n^* + \delta u$$

$$\bar{g}_n \equiv -T_n^* + \delta v$$

inserting into Eq. (33) and neglecting terms of higher order in δ, we obtain

$$u + \bar{x} v = (\bar{x}\, T_n^*)''$$

$$v'' + \bar{x} u = 0$$

from which

$$\bar{x}^2 v - v'' = \bar{x}(\bar{x}\, T_n^*)'' = \bar{x}^4 T_n^* - \bar{x}^{n+2} + 2\bar{x}\, T_n^{*\prime} \tag{34}$$

The solution of this equation is given in Ref. 7, Table 4:

$$v = \frac{1}{16} \begin{cases} 1 - 5\bar{x}^2 T_0^* - 2\bar{x}^3 T_0^{*\prime} - 10 U_0 & (n = 0) \\ 3\bar{x} - 5\bar{x}^2 T_1^* - 2\bar{x}^3 T_1^{*\prime} - 10 U_1 & (n = 1) \end{cases} \tag{35}$$

Equation (35), where v is expressed by means of tabulated functions, is asymptotically correct for $\delta \to 0$, that is, $\rho^* \to 1$. Corresponding formulae for u, thence $\bar{f}_n$ and $\bar{g}_n$, thence f_n and g_n, and finally T_n follow directly; again, $\bar{A}$ is determined by Eq. (12). We list here some characteristic results:

$$\sqrt{\rho}\, f_A'(0) = c_0 - (3 - v_0)\delta \quad ; \quad g_A(0) = -\sqrt{\rho}\,(c_0 - v_0\delta) \quad .$$

$$f_B(0) = -2c_1\delta \quad ; \quad g_B'(0) = \sqrt{\rho}\,(c_1 - v_1\delta) \quad .$$

$$\sqrt{\bar{A}} = c_0 - \delta(3 - v_0) \quad ; \quad \bar{B} = \delta \bar{A}^{3/2}$$

$$-T_0''(0) = \frac{1}{c_0^2}\left[1 - \left(\frac{10}{3}\, c_0 - \frac{2(3 - v_0)}{c_0}\right)\delta\right]$$

$$T_1'(0) = \frac{c_1}{c_0}\left[1 - \left(\frac{2 + v_1}{c_1} - \frac{3 - v_0}{c_0} - 2c_1\right)\delta\right] \qquad (36)$$

The constants that appear here are

$$c_0 \equiv T_0^*(0) = 1.31103 \quad ; \quad c_1 = T_1^{*\prime}(0) = 0.59907$$

$$v_0 \equiv -v(0) = \frac{1}{16}(10\, U_0(0) - 1) = 0.8066$$

$$v_1 \equiv v'(0) = \frac{1}{16}(3 - 10\, U_1'(0)) = 0.0281 \qquad (37)$$

The asymptotic formulae Eq.(36) agree, within the expected accuracy, with the numerical values available for $\rho = 15$ (from Ref. 5 and from our more accurate computer results, Appendix A). The limit tangents to the ψ-functions in Fig. 4 are

$$\frac{d\psi}{d\rho^*} = -\frac{3}{8}\frac{d\psi}{d\delta} \approx \begin{cases} 2.40 & \text{for } -T_0''(0) \\ 2.03 & \text{for } T_1'(0) \end{cases}$$

The foregoing results allow a ready proof of a point that was made in Ref. 1. Figure 6 of Ref. 1 shows the nondimensional torus stiffness

$$S^* = \frac{1}{c}\left[\frac{\bar{A}}{\sqrt{\bar{B}}} + 2\sqrt{\bar{B}}\,T_1'(0)\right]$$

(compare Eq. (38) below) over $p_0/p = 0.7/\rho$. Now $\bar{A}$, $\bar{T}_1'(0)$ and c are all of the form $a_0 - \delta a_1$, while $\bar{B} \sim \delta$. Thus $S^* (p_0/p)^{3/4}$ is of the form $S_0 + (p_0/p)^{3/2} S_1$ and, plotted over p_0/p, has a horizontal tangent at the membrane limit (furthermore, the contributions to S_1 of the two terms in S^* have opposite signs and tend to cancel each other). It follows that the result of membrane theory remains asymptotically valid for finite shell thicknesses h.

As an illustration, assume, as in Appendix C, that the thickness h of a given torus shell is being varied, and that p is varied simultaneously such that the mean stress $E\,\epsilon_0$ remains constant. Then $\delta \sim h^2$, and the actual (dimensional) shell stiffness takes the form $S = a_0 h + a_1 h^3$. The term $a_0 h$ here is the result of membrane theory; the second term is negligible if h is small (Ref. 1, Fig. 7).

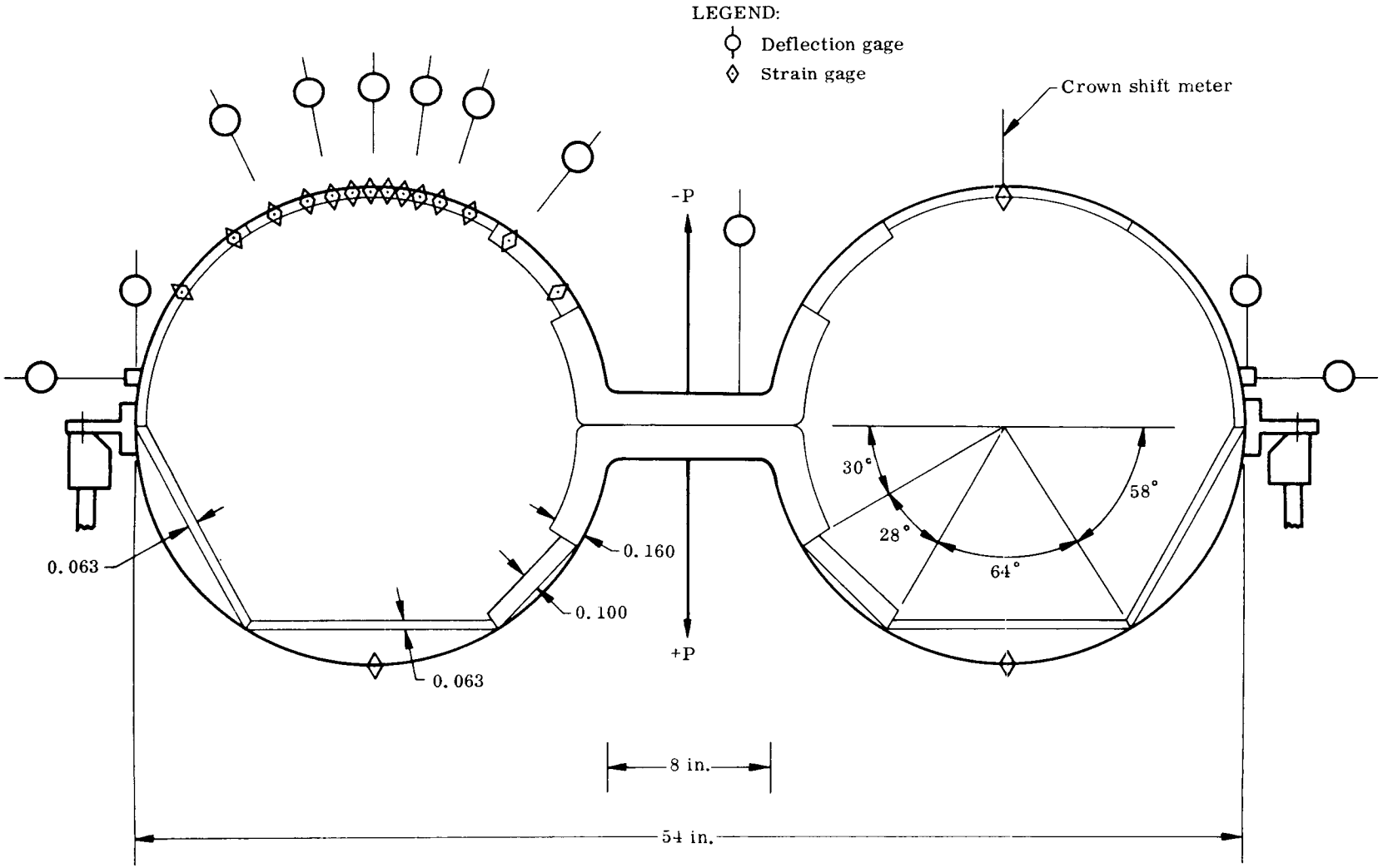

Fig. 5. Experimental Model and Test Arrangement

III. COMPARISON WITH EXPERIMENTAL RESULTS

1. Survey

The test program is described in more detail in Appendix B. Figure 5 is a schematic drawing of the model: a complete circular torus shell made by explosive forming of a preform welded from flat aluminum sheets. The analysis refers to the actual measurements of the middle face of this shell;* these are

overall diameter $D = 2R(1 + a) = 54.4$ inch
meridional radius $R = 11.5$ inch
opening ratio $a = 1.365$

The actual mean shell thickness at the crown is $h = 0.0627$ inch; thus $R/h = 183$.

The model shell was supported at its outer rim, was pressurized to eight levels of the internal pressure p, between $p = 0$ ($\rho = 0$; $k = 7.42$) and $p = 30$ psi ($\rho = 3.36$; $k = 5.94$) and, at each pressure level, was loaded by an axial force P, both upward and downward. Three levels of load intensity were applied at each pressure p, selected to produce axial deflections of about 1/16 inch, 1/8 inch and 1/4 inch. The overall stiffness of the shell was found to be practically independent of the load level. Certain nonlinearities of the detailed shell behavior occurred; these will be discussed.

The main model instrumentation consisted of strain gages and deflection gages on one meridian of the upper half-shell. The thickness at the crown here is 0.0615 inch. The strain measurements have been transformed into shell stresses and moments. The elastic constants

$E = 1.07 \times 10^7$ psi (from our coupon tests)

$\nu = 0.32$ (Poisson ratio)

were used in this transformation.

Where applicable, the effects of pressurizing the shell and of applying an axial load to a pressurized shell will be considered separately. In the presentation of the results of applying a load, this load will always be assumed to be

*Figure 5 gives nominal measurements.

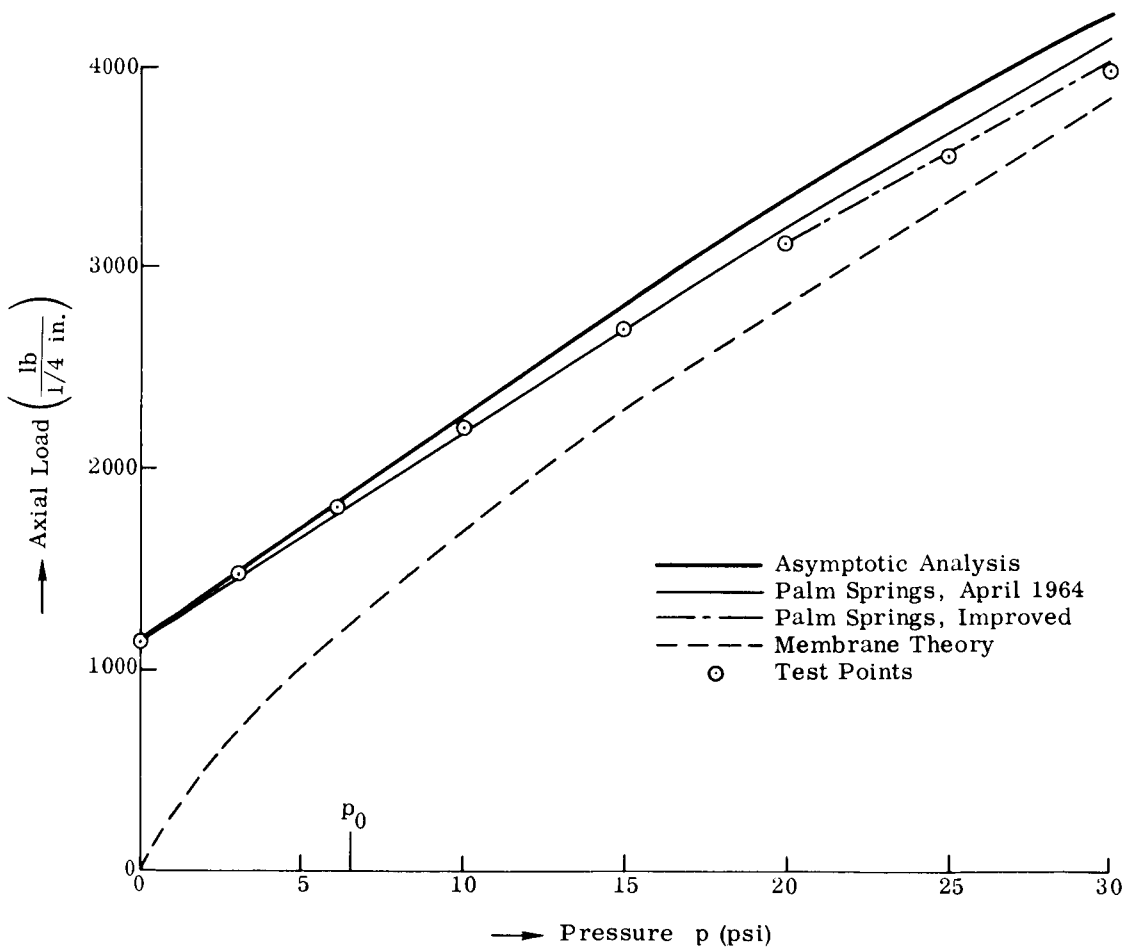

Fig. 6. Stiffness S Under Axial Load

directed downward, as in Fig. 1; the effect, measured on the upper half-shell, of applying an upward load will be interpreted as the effect on the lower half-shell of applying a downward load.

Two types of comparisons with analytical results will be made. The analytical predictions for the three most significant quantities, namely, overall axial stiffness S, crown shift x_0 and crown ring force $N_{\theta 0}$, were evaluated throughout the range of applied internal pressures. On the other hand, where local stresses and displacements are presented along the shell meridian, only the analytical result for $\rho = 1$ (that is, p = 8.92 psi) will be shown.

The analytical results shown are those that arise from the asymptotic theory that is discussed in Chapter II. In a few cases, the correction that would be obtained by evaluating more complete shell equations has been estimated and will be indicated.

2. Stiffness, Crown Shift and Crown Ring Force

The asymptotic formula for the overall stiffness S under axial load is (Ref. 1 Eq. (48))

$$S = \left[\frac{\bar{A}}{\sqrt{\bar{B}}} + 2\sqrt{\bar{B}}\, T_1'(0) \right] \frac{\pi E h^2}{cR\sqrt{3(1-\nu^2)}} \qquad (38)$$

Figure 6 shows S as predicted by Eq. (38) together with measured stiffnesses.

In Fig. 6, S is given in terms of the load P that is required to produce a central axial deflection of 1/4 inch. In the case of the test results, actually applied load and measured central axial deflection have been referred to this standard deflection of 1/4 inch. This procedure was used to evaluate all load effects; that is, all load curves shown below are referred to the same standard deflection. (In general, the results shown are those obtained from the tests with the highest applied load, i.e., the tests with a nominal deflection of 1/4 inch).

The important role of the pressure stiffness is clearly demonstrated by Fig. 6. The initial model stiffness is about doubled by applying an internal pressure p = 11 psi. Conversely, extrapolating to the left, one recognizes that an external pressure $p \approx 11$ psi would reduce S to zero.

The pressure $p_0 \approx 6.5$ psi is that pressure where, in the analysis, the contributions from pressure stiffness and bending stiffness (the two terms in the bracket of Eq (38)) are about equal, and might be considered to be the center of the transition range. The bending stiffness contribution, which is 100% for $p = 0$, has already decreased, not only in its relative but also in its actual magnitude, as p_0 is reached, and decreases further as p is increased beyond p_0.

Several analytical results are shown. "Asymptotic analysis" arises from Eq. (38) with accurate values of $\bar{A}$, $\bar{B}$ and $T_1'(0)$. For the "Palm Springs" curve, taken from the earlier version of Ref. 1, $\bar{A}$, $\bar{B}$ and $T_1'(0)$ had been calculated by an approximate method; by coincidence, this approximation fits the test points even better than does the accurate curve. "Improved" refers to a correction (of relative order $1/k^2$) that is given in Ref. 1 as resulting from evaluating the membrane equation in a more complete formulation (Ref. 2). The same improvement should also be applied to the accurate curve. When this is done (not shown in Fig. 6) the maximum difference that remains between test and "corrected accurate" analysis is 4%.

The curve "Membrane theory" is the result of neglecting the shell bending stiffness in the analysis; it is added as an illustration. In it, the "improvement" has been incorporated.

In judging the degree of agreement that is shown in Fig. 6, one has to recall that even the "more complete formulation" (Ref. 2) is not exact but allows errors that may also reach the relative order $1/k^2$. Considering further the uncertainty of determining experimental parameters, the agreement between theory and experiment as shown in Fig. 6 is as good as can possibly be expected. In fact, the accuracy of the analytic prediction that is achieved in Fig. 6 for an integral quantity, the axial stiffness, can hardly be expected in all details. This is illustrated by Fig. 7, where the crown shift x_0 is shown.

As the shell is pressurized, its crown moves inward (toward the axis) by the distance $x_{00}R$; as an axial down load is applied to produce an axial

deflection $\Delta \cdot R$, the crown moves outward by $x_{01}R$ on the upper half-shell, and moves further inward by $x_{01}R$ on the lower half-shell. The total crown shift, thus, is

$$x_0 = -x_{00} \pm x_{01}$$

The analytical predictions are

$$x_{00} = \frac{\epsilon_0 \, k \, \pi}{4c \sqrt{a^2 - 1}} \quad ; \quad x_{01} = \frac{\Delta k}{2c} \tag{39}$$

Figure 7 shows, firstly, that x_{00}, the crown shift due to pressure, analytically predicted to be quite small, was measured an order of magnitude larger. This does not, however, imply a failure of the analysis; it simply demonstrates a consequence of a local imperfection of the shell. In our test arrangement, the meridian where strain gages and crown shift meter were to be fixed had to be diametrically opposed (Fig. 5) and had to be situated symmetrically removed from the meridional welds. After allocating the more perfect one of the two available meridians to the strain gages, we were forced to fix the crown shift meter at a place where the shell had a local imperfection, Fig. 8. Thus the crown shift meter (which measured the rotation β of the shell point $x = 0$ rather than the actual movement of the crown) did not in fact measure the analytical quantity x_{00} but measured instead the straightening out of a local imperfection by the internal pressure p.

In spite of this local imperfection, good agreement between theory and test was obtained for the crown shift x_{01} due to load; in fact, evaluation of the more complete shell equation would move the analytical curve down by about 2% at p = 30 psi and would thus yield an even better agreement. This observation will be seen to be generally true; imperfections of the shell may strongly affect the reaction of the shell to internal pressure, but have only little effect on the reaction of the pressurized shell to an axial load.

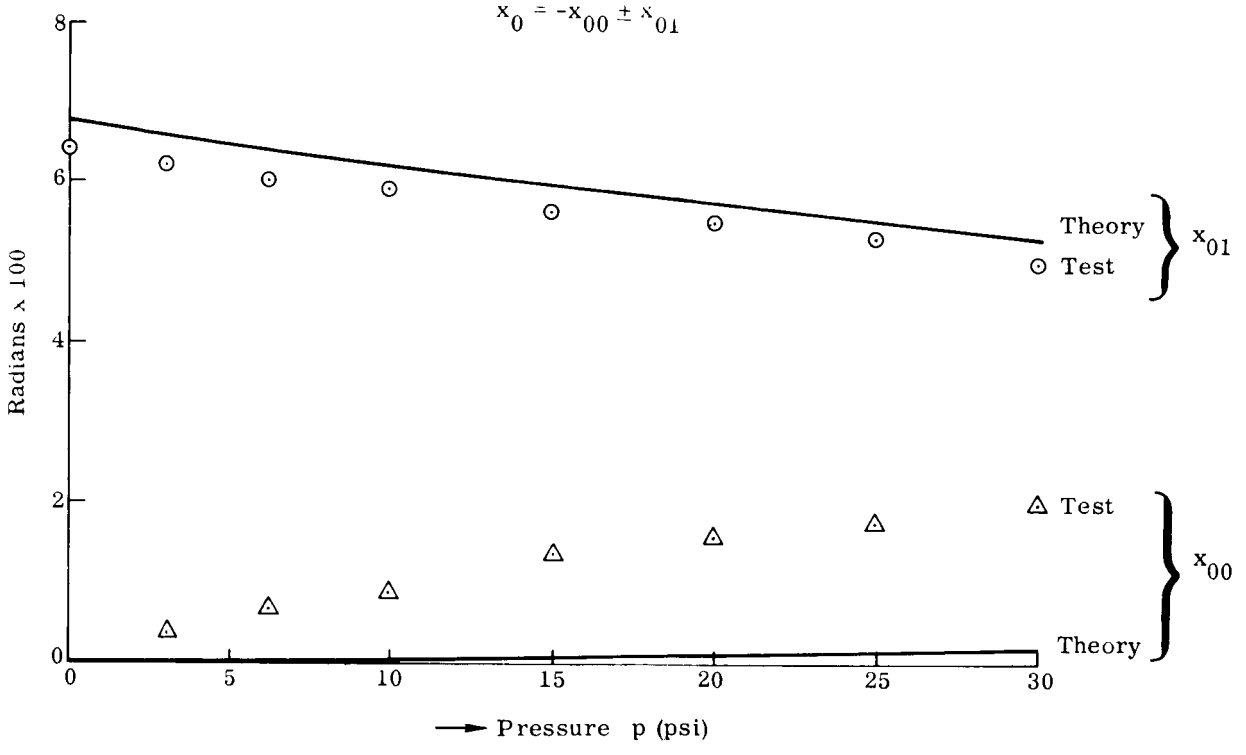

Fig. 7. Crown Shift x_0

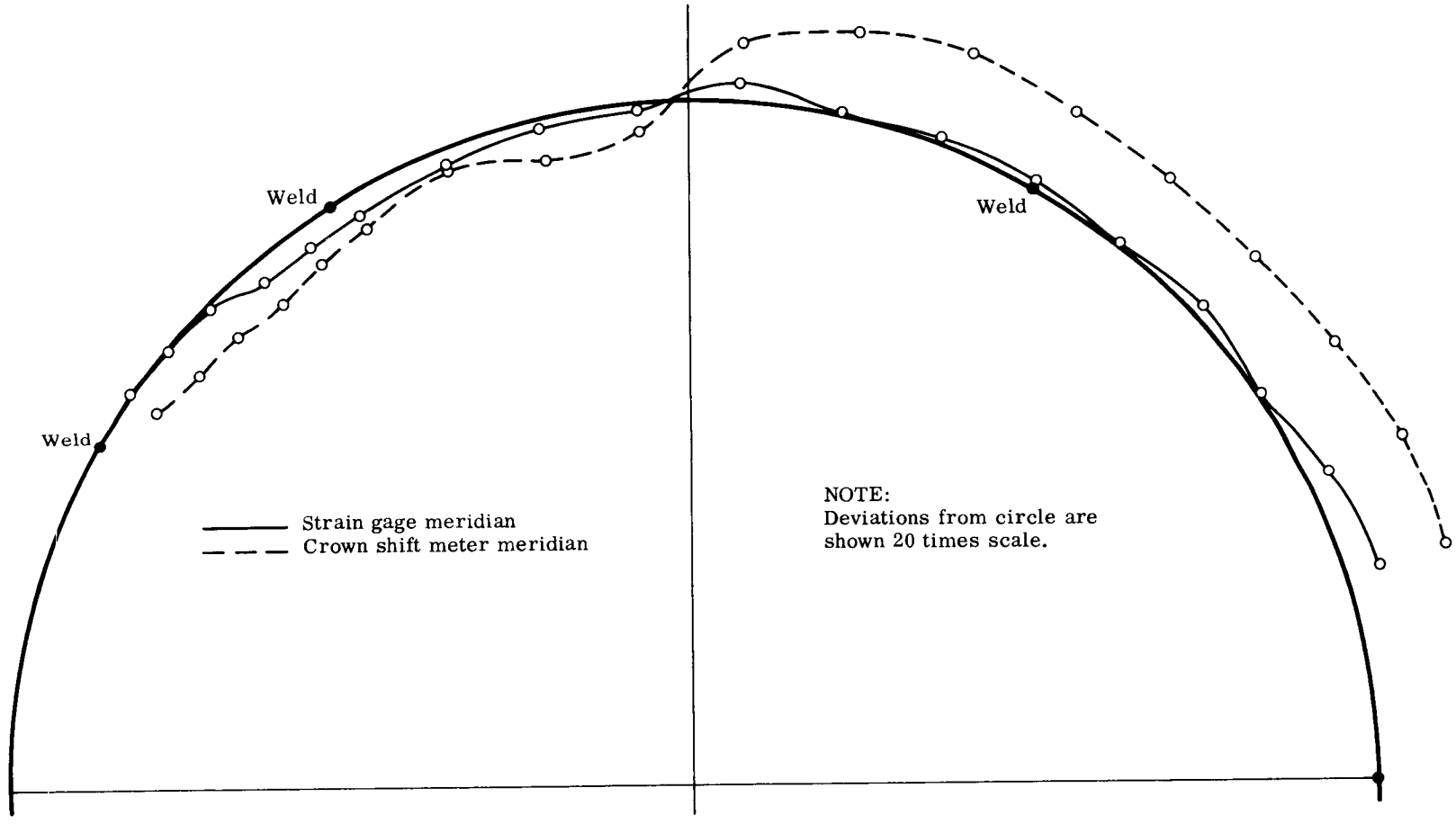

Fig. 8. Meridian Imperfections

A significant observation in Fig. 7 is that x_{01} varies relatively little between p = 0 and p = 30 psi, in a pressure range where the stiffness S increases very considerably, Fig. 6. Indeed, the number c in Eq. (39) is practically a constant, see (16); the change in x_{01} that is seen in Fig. 7 illustrates the decrease of the number k as p is increased.

Figure 9 shows the ring force N_θ at the crown point x = 0. Pressurization alone produces a tension force N_θ which does not differ much from the result $N_\theta = pR/2$ of linear membrane theory. An axial down load adds compression at the upper, tension at the lower crown. These additional crown stresses become the critical design stresses if the axial load is sufficiently large; in particular, they might produce buckling of the upper crown. Analysis predicts*

$$N_{00} = \frac{pR}{2} - \left[pR\,a\,k^2\,T_1'(0) + \frac{2EhB}{a}\,k^4\,|\,T_1'''(0)\,| \right] x_0 \qquad (40)$$

It is seen from Fig. 9 that the ring force due to load increases considerably less with increasing pressure than does the axial load, Fig. 6.

The agreement between theory and test, excellent in the case of the pressure effect, is not more than fairly good at high pressures in the case of the load effect. Here evaluation of the more complete shell equations would move the theoretical curve down slightly, but not enough to produce complete agreement. On the other hand, control strain gages that had been placed at the insides of other crown positions, Fig. 5, measured higher strains under load at high pressures. It seems that the steep local maximum of the ring force N_θ that occurs at the crown, see below Fig. 10b, is more sensitive than other effects of the axial loads. Indeed, the measured $N_{\theta 0}$ was somewhat nonlinear with respect to load; this, perhaps, indicated a shift of the maximum ring force as the actual crown moved; see below. The test points in Fig. 9 have been obtained by interpolating for zero axial load, in accordance with the assumptions of the analysis. The actual maximum load produced slightly smaller central ring forces $N_{\theta 0}$, see Fig. 10b.

---

*In the limit $\rho^* = 0$, both Eq. (40) and Eq. (38) agree with the results of Clark[4].

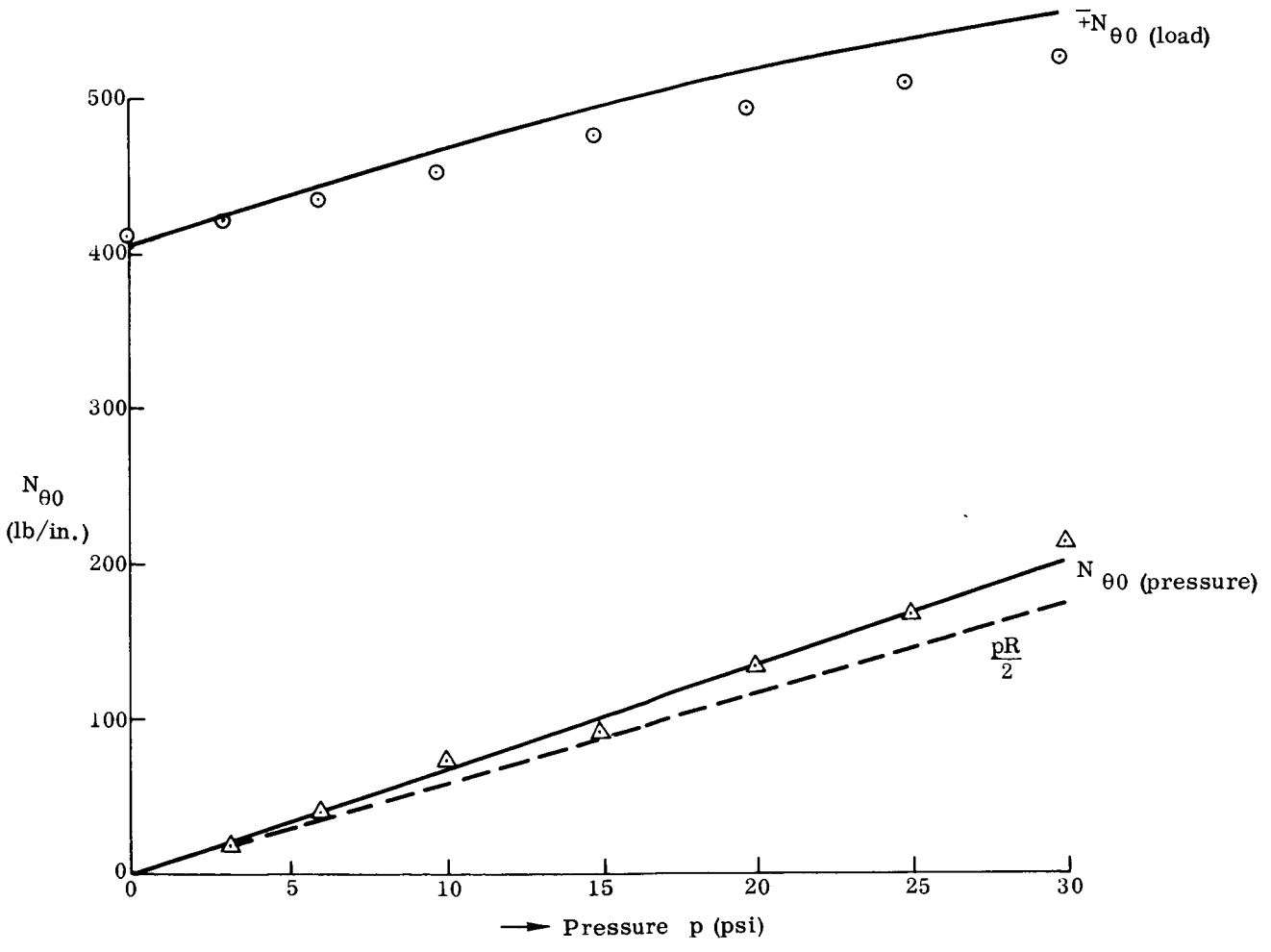

Fig. 9. Ring Force at Crown

3. Stresses and Bending Moments

Figures 10 and 11 show direct stresses and bending moments. Of the test results, only those for multiples of p = 10 psi are shown, and curves between test points have been drawn only where this helped the presentation. In Figs. 10a and 11a (pressure only) double points are sometimes shown; these refer to tests on two different days and thus indicate the degree of reliability of the test results. In Figs. 10b and 11b (stresses due to loads) only results for the upper half-shell are usually shown.

In the diagrams, $\sin \phi_0$ is the abscissa, and the torus axis is to the left. In each case, one analytical curve is given; this curve refers to $\rho = 1$, p = 8.9 psi, as aforesaid, and should be compared with the test results for p = 10 psi.

In Fig. 10a (pressure only) the test points for the meridional stress N_ϕ agree closely with the results of linear membrane theory - as they should according to Ref. 2. An exception occurs at $\sin \phi_0 = -0.6$. At this strain gage point, the shell thickness is increased to h = 0.101 in.; it lies about 8 shell thicknesses away from the weld at $\sin \phi_0 = 0.53$. Neither observation seems to explain the somewhat high stress that was here measured (compare also Fig. 11a). (However, in a region away from the crown that is not of primary concern here.)

The test points for N_θ in Fig. 10a show the predicted type of behavior. The deviation from linear membrane theory, predicted to be 18% for a = 1.5 in Ref. 2, is slightly larger here because the opening ratio a is somewhat smaller.

In Fig. 10b (load effects) N_ϕ is always quite small, and the agreement between theory and test is as good as could be expected. The ring stress N_θ is much larger; in general, the agreement between theory and test is good. At the left, curves connecting test points for p = 0 and p = 30 psi are drawn. These curves show an increasing wave length with increasing pressure, indicative of the corresponding decrease in k and, therefore, increase of the width of the crown range.

The experimental stresses N_θ at the center $\phi_0 = 0$ appear to be slightly low; partly this is due to the fact that in Fig. 10b, as distinct from Fig. 9, the actual experimental stresses at maximum load are shown.

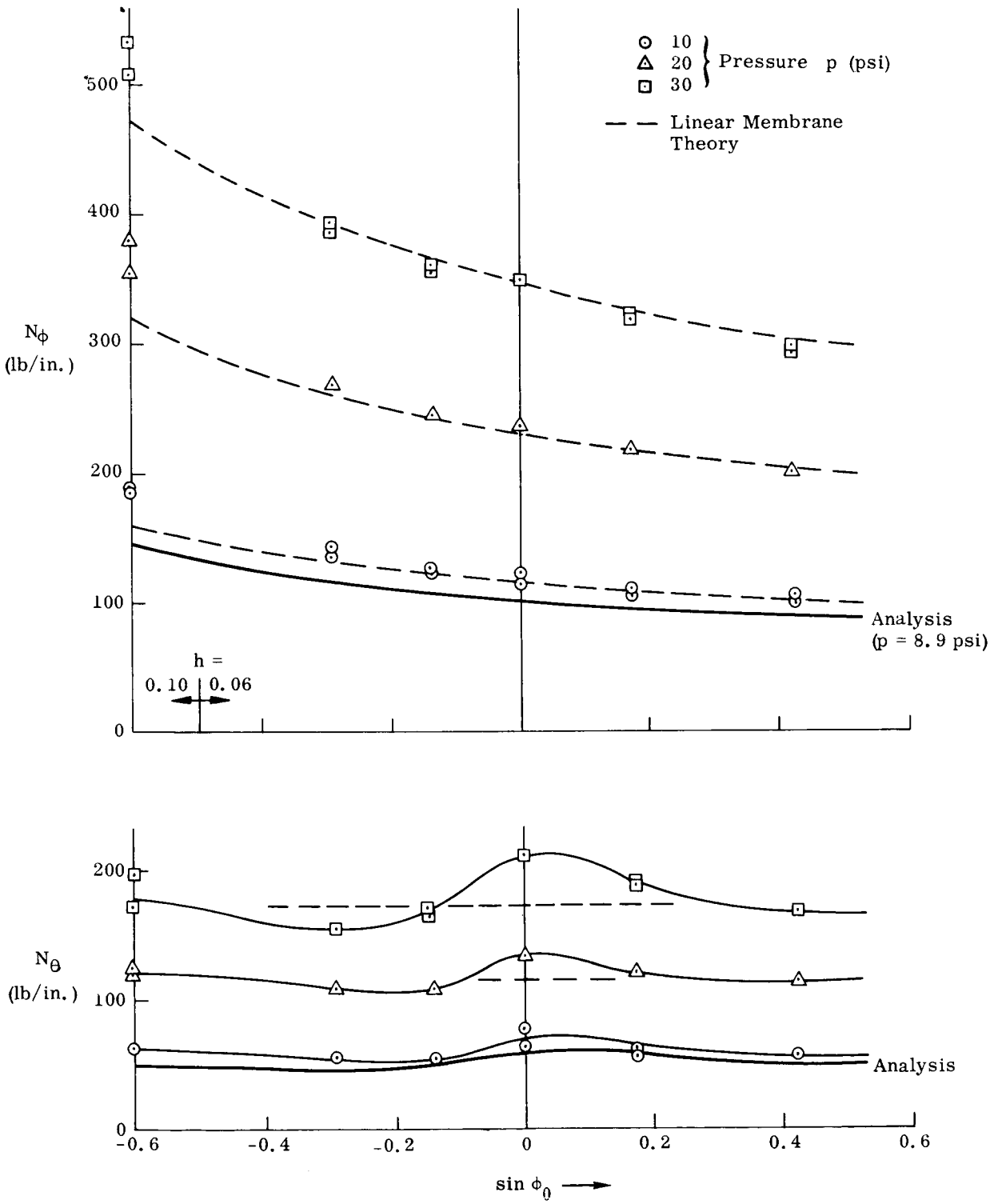

Fig. 10a. Direct Stresses Due to Pressurization

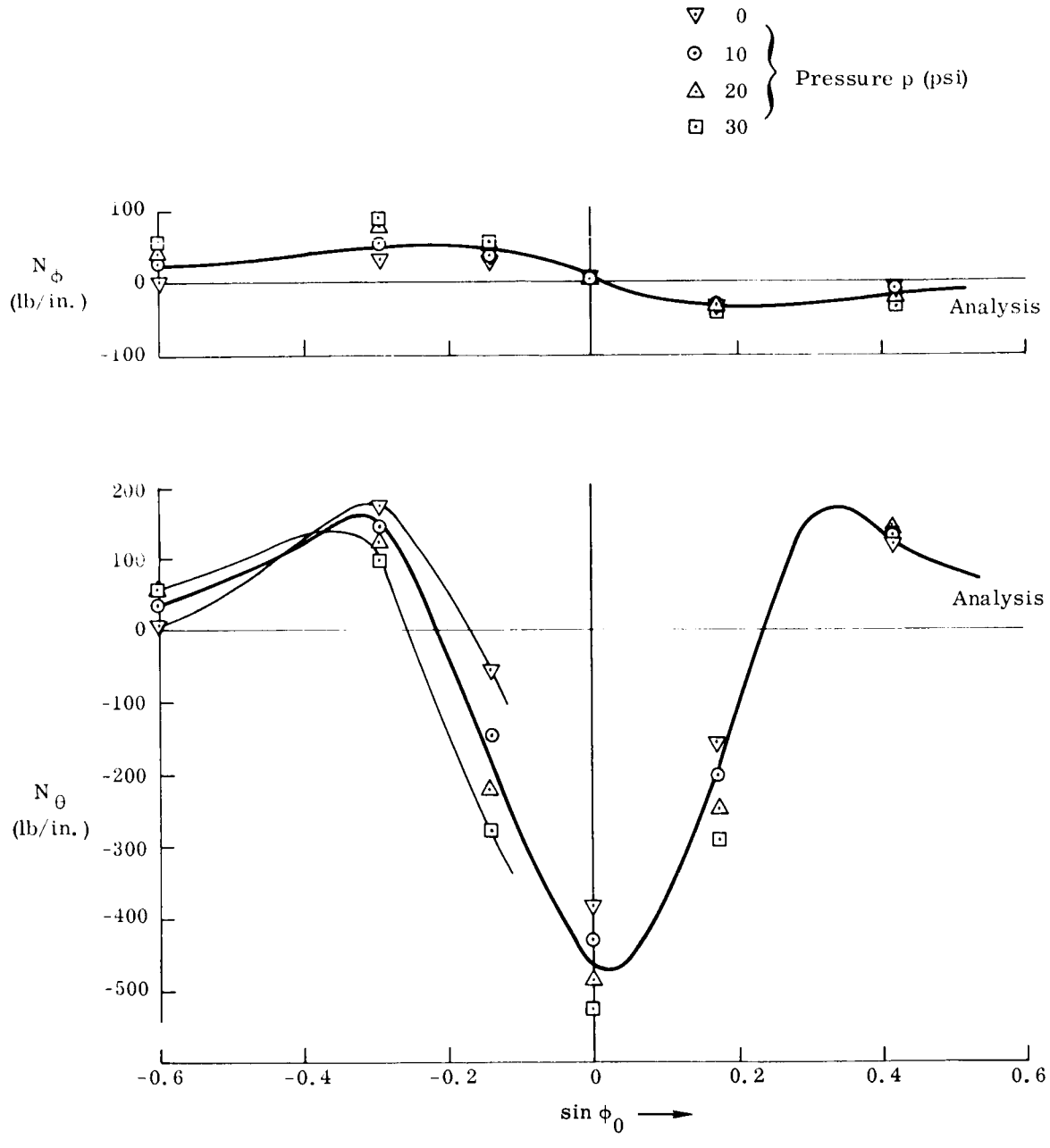

Fig. 10b. Direct Stresses Due to Axial Load

In this connection we should first turn to Fig. 11b, the bending moments due to axial load.* Here, for both M_ϕ and M_θ, the test points for p = 10 psi, upper half-shell, have been connected by continuous curves. While general character and amplitude of theoretical and experimental curves agree fairly well, there is a distinct phase shift toward the right in these experimental curves. On the other hand, the test results for the lower half-shell, which are indicated by dashed curves, show a corresponding (but lesser) phase shift to the left.

Investigating this phase shift, we found that it varies linearly with the axial load, and that the apparent contradicting between theory and experiment is removed by a combination of a hypothesis (1) and an observation (2):

(1) The effective initial crown point in the range of the strain gage meridian was displaced from its nominal position outward by $\Delta\phi \approx 0.025$ (that is, by a distance $R\Delta\phi \approx 0.3$ inch).

(2) As the shell crown shifts due to the application of an axial load (crown shift x_{01}) the bending moment distribution tends to move with the crown. This is a nonlinear effect; the (quasilinear) analysis had to assume that x_{01} is infinitesimally small.

The imperfection that is assumed in (1) is not indicated by Fig. 8 but, as an imperfection that may be an average over a range of meridians, it is within the practically achievable manufacturing tolerance. Indeed, Fig. 11a, bending moment due to pressurization, might be indicative of a local deviation from exact axial symmetry. Note that the scale of Fig. 11a is ten times the scale of Fig. 11b; the measured bending moments are actually quite small. They

*For the calculation of the bending moments, two sets of formulae were available: the accurate formula according to the Kirchhoff hypothesis, Ref. 1 Eq. (20), and its simplified (Donnell-type) form, Ref. 1 Eq. (22). As expected, there were noticeable differences in the moments calculated from the different formulae, but only in the moments due to pressurization, Fig. 11a, which were small themselves. Here the difference amounted to about 13% of the maximum value of M_θ. (As shown in Ref. 1, these differences will cancel out on insertion in the shell equations.)

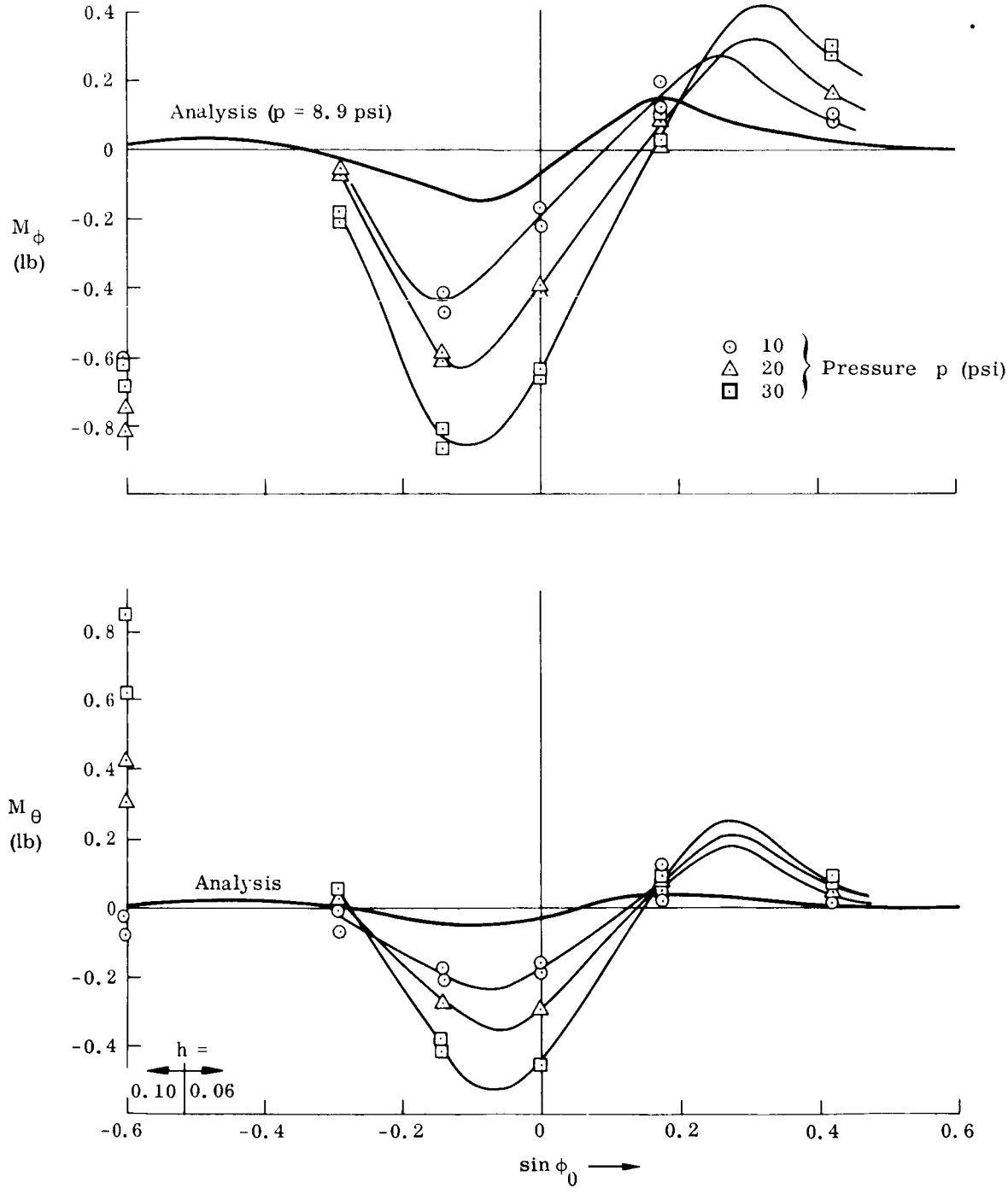

Fig. 11a. Bending Moments Due to Pressurization

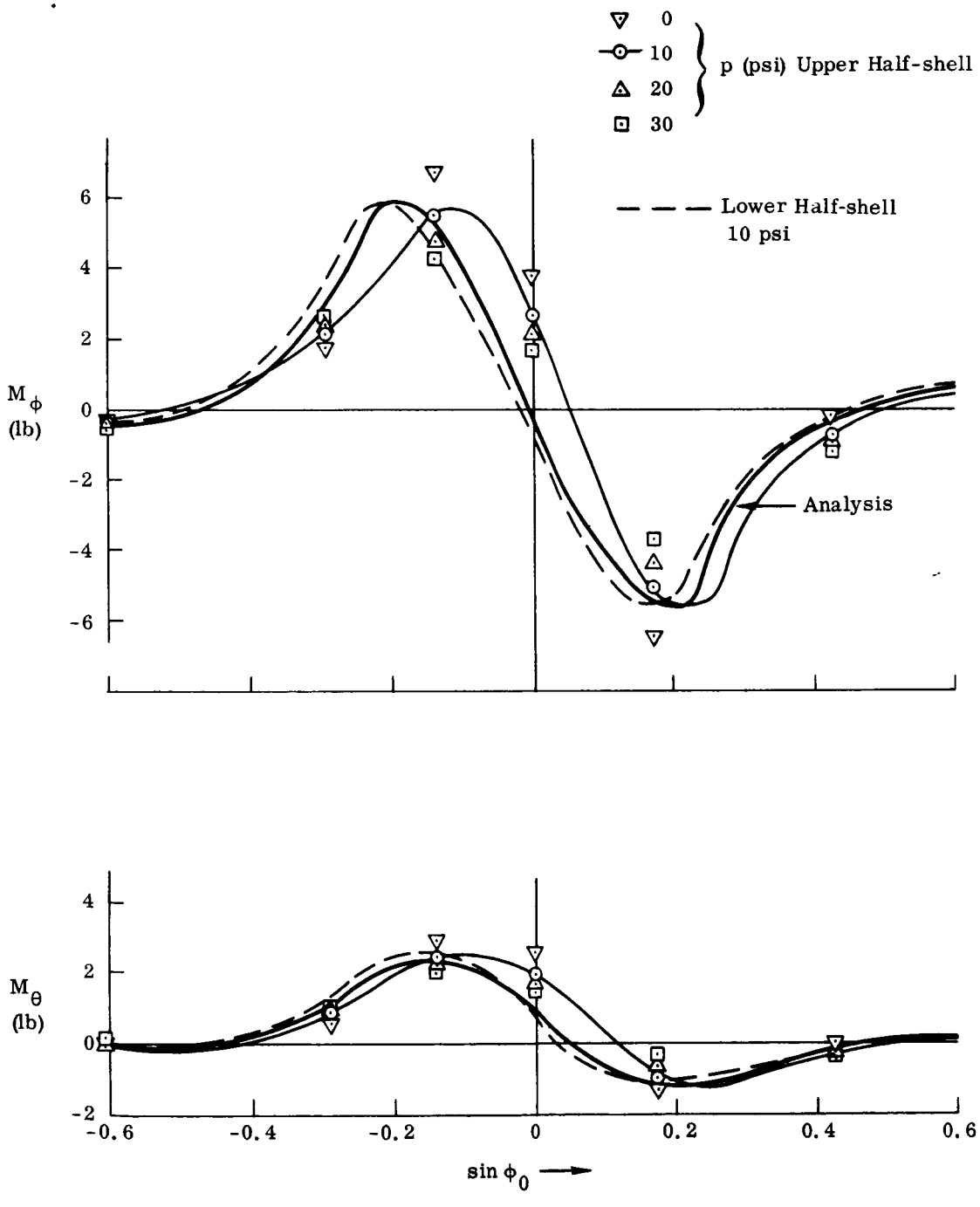

Fig. 11b. Bending Moments Due to Axial Load

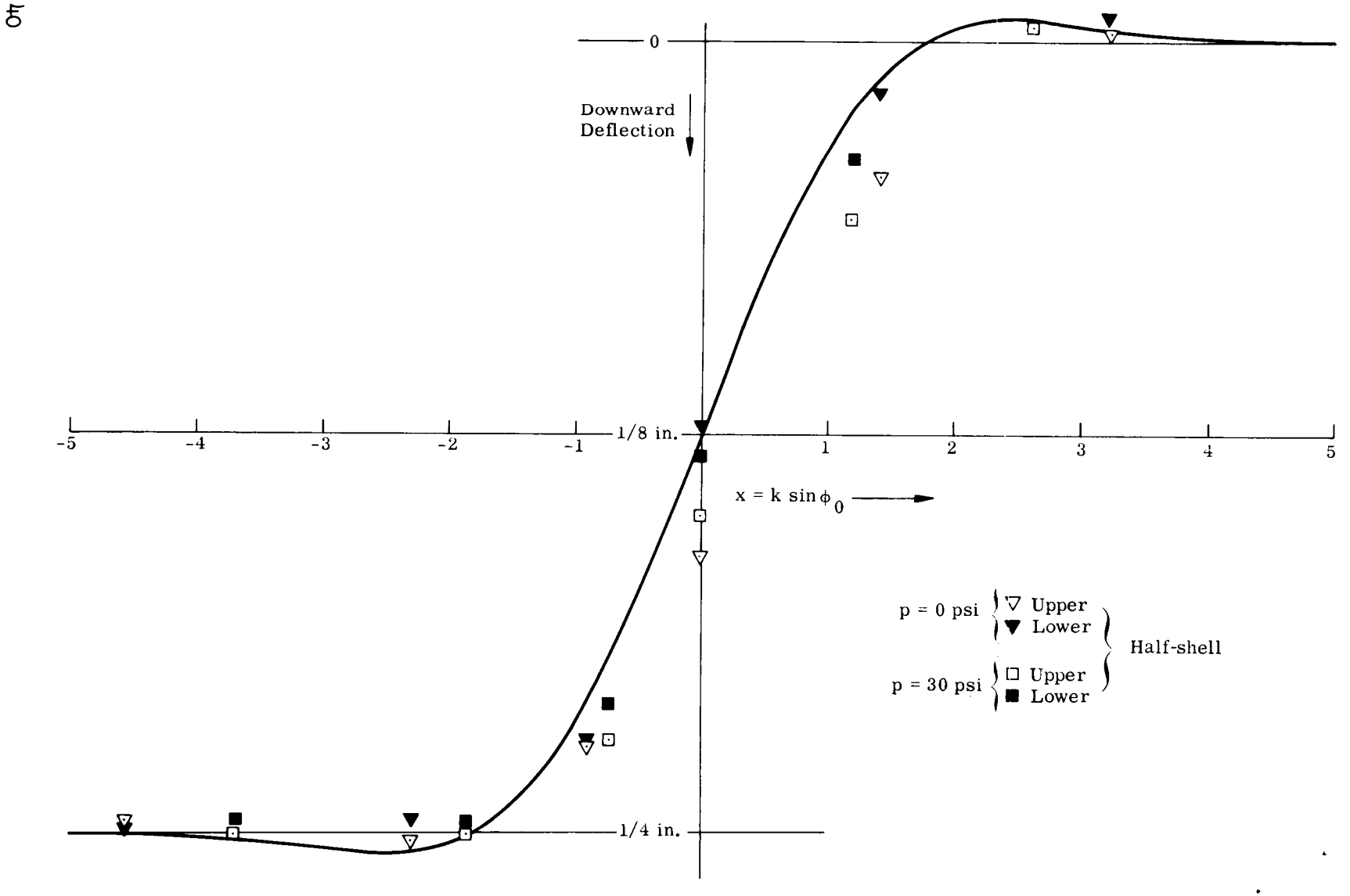

Fig. 12. Vertical Deflections

are, on the other hand, considerably larger than the predicted bending moments. In this respect, the situation described by Figs. 11a and 11b corresponds to the relation between test and analysis in Fig. 8 for the two crown shift contributions x_{00} and x_{01}.

4. Local Shell Deflections

The local vertical shell deflections were measured along a shell meridian that was close to the strain gage meridian. Only the deflections due to axial load at p = 0 and p = 30 psi are shown in Fig. 12 (the deflections due to pressure only were too small). They were measured at fixed shell locations sin ϕ_0 but are plotted over x = k sin ϕ_0 rather than over sin ϕ_0; this led to the horizontal displacement in Fig. 12, between p = 0 and p = 30 psi, of corresponding test points. It is readily seen that this horizontal displacement tends to make the test points for each half-shell fall on one curve. Indeed, the analytical deflection curve, shown in Fig. 12 for $\rho = 1$, varies very little between $\rho = 0$ and $\rho = \infty$, owing to the close similarity of the T_1 - functions in Fig. 3.

Furthermore, the test points indicate a horizontal shift corresponding somewhat to the one discussed above in connection with Fig. 11b. Note that an initial crown displacement $\Delta\phi \approx 0.025$ means $\Delta x \approx 0.18$ for p = 0 and $\Delta x \approx 0.15$ for p = 30 psi in Fig. 12.

IV. IMPROVEMENT OF THE ASYMPTOTIC SOLUTION

Equation (1), the starting point of the asymptotic analysis, arises from the quasi-linear theory, Ref. 1, by developing the two differential operators which respectively represent pressure stiffness and bending stiffness in series in descending powers of k, Eq. (6), and neglecting all terms but the first one in each series.

An improved analysis arises if also terms of relative order $1/k$ in the stiffness operators are considered. These are the terms which have the coefficients d and e in Eq. (6), and corresponding coefficients $\tilde{d}$ and $\tilde{e}$ in the bending stiffness operator. The amended operators replace T_n'' and $\bar{T}_n^{IV}$ in Eq. (9); thus modified, Eq. (9) defines improved basic functions T_n^1 which may be written as

$$T_n^1 = T_n + \Delta(d, e, \tilde{d}, \tilde{e})/k$$

As defined so far the corrective function Δ itself contains terms with $(1/k), \cdots$ but, in order to be consistent, we should discard these higher order terms; that is, we should replace Δ by its asymptotic limit for $k \to \infty$. Doing this, we find that T_n^1 takes the form

$$T_n^1 = T_n + (d\delta + e\epsilon + \tilde{d}\tilde{\delta} + \tilde{e}\tilde{\epsilon})/k \qquad (41)$$

in which δ, ϵ ... are influence functions for the individual coefficients d, e... These influence functions, just as the functions T_n themselves, are well defined functions of x and of the transition parameter ρ^*, and may be tabulated once and for all.

There are four such functions for each n in the transition range itself; the required number reduces to two at each limit. In Ref. 7, where this "influence function method" is discussed in detail for the limit case $\rho^* = 1$ (i.e., the membrane) the influence functions δ and ϵ that are required in this limit have been tabulated. In Ref. 7, the method is followed through, by including

terms of higher order in (1/k), in an investigation of the convergency of the method. These higher order terms involve increasing numbers of influence functions. However, in practical applications only the first order influence functions will usually be considered, and the subsequent remarks will be restricted to these.

It is shown in Ref. 7 that the influence functions are relatively small compared with the T_n, and converge to zero more rapidly than T_n as $|x| \to \infty$. Thus, as the coefficients d, e.. are of order 1/a, and as k is supposed to be large, the corrective term in Eq (41) is relatively small a fortiori. This is the reason why the asymptotic analysis, Chapter II, is often sufficiently accurate for practical applications, Chapter III.

The influence method was first developed in Ref. 7. The method of Refs. 3, 4 and 5 is characterized by the use of a transcendental transformation of Liouville type, with the aim to absorb the terms of order (1/k) into transformed forms of function T_n and coordinate x. However (apart from involving undesirable numerical complications) this method requires that x be small. Thus, for $x = 0$ the result of the transcendental transformation will agree, in its terms of order (1/k), with the (exact) result of the influence function method, but it will not necessarily be correct (even in its terms of order 1/k) for x large.

The comparison between the two results is shown in Fig. 8 of Ref. 7 (where the higher order terms in the result of the transcendental transformation have been eliminated in order to simplify the comparison). It is found: the transcendental transformation yields the correct result for all values of x in the case of the influence function ϵ, but only for $x = 0$ in the case of the influence function δ.

It follows that the influence function method, apart from being simpler in its application, is also more accurate.

Preliminary considerations show that, like the functions T_n, the influence functions should vary little as the transition parameter ρ^* is varied. One point should be mentioned, however: it is shown in Ref. 7 that the influence functions

for $\rho^* = 1$ are closed form expressions in terms of the T_n. This does not seem to be the case for arbitrary values of ρ^*. In consequence, it appears that determination by means of numerical integration will be required.

So far we discussed methods of improving the asymptotic solution in the range of the shell crown. A different type of problem arises from the fact that away from the crown the asymptotic solution converges toward the membrane solution. Shell boundary conditions may be given which are not fulfilled by the membrane solution. This poses no new problem if crown range and shell boundaries are sufficiently far apart, so that one has to deal with separate boundary layer problems. The required homogeneous solutions of Hankel type will be oscillatorily convergent as far as they are determined by bending stiffness (compare e. g., Ref. 8) but will be monotonically convergent as far as they are determined by pressure stiffness (Ref. 7).

If crown range and boundary layer interact, direct numerical integration (Appendix A) appears to be indicated. This will be the case in particular if the shell opening parameter a is large. The coefficients d, c $\cdots$ to the terms of order 1/k will be small in this case, and in this sense the asymptotic analysis would seem to become more accurate; however, k decreases as a increases, and in consequence the width of the crown range grows. The asymptotic analysis becomes meaningless if the crown range is no longer small but covers the whole of the shell.

V. CONCLUSIONS

The asymptotic analysis of the mechanism that develops at the free crown of torus-type pressurized shells of revolution, previously developed in Ref. 1, has been brought into a form where the solving functions, T_n, vary only little in the transition from the shell without internal pressure ($\rho^* = 0$) to the pressurized membrane ($\rho^* = 1$). Relations to and between previous publications have been established, and the transition from the fourth order problem ($\rho^* < 1$) to the second order problem ($\rho^* = 1$) has been discussed quantitatively in some detail (Chapter II).

The asymptotic analysis should be adequate if the crown range, measured in terms of the length R/k, is reasonably small compared with the meridional dimension of the shell. This is confirmed by a comparison with test results, Chapter III, where $k \approx 6$ or 7. In this comparison, the effects of pressurizing a torus shell and of applying an axial load to a pressurized shell are considered separately. The primary effects of pressurization are the direct forces, N_ϕ and N_θ. These are adequately predicted. On the other hand, crown shift x_{00} and bending moments M_ϕ and M_θ, all of which are quite small, have been found to be very sensitive to small, and practically unavoidable, deviations of the actual shell from its design ideal.*

Axial load produces both forces and moments. All of these are adequately predicted if the load is small; so are the vertical shell deflections. If the axial load is sizeable, then the system of shell stresses and shell deflections has a tendency to move with the shell crown as the latter moves, due the application of the load. This nonlinear effect, which does not, however, seem to affect the overall magnitude of the stresses and deflections, cannot be predicted by the quasi-linear theory.

The effects of axial load have been presented referred to a standard overall shell deflection rather than a standard load. With the deflection standardized, the crown shift under load, the shape of the shell deflection and the ring force

*The critical operation in trying to manufacture an accurate circular torus shell was the welding together of the two half-shells (Appendix B).

N_θ are all relatively little affected by the internal pressure p, even though the required axial load (i.e., the shell stiffness) increases considerably as p is increased.

The asymptotic analysis will usually be adequate for space type structures, and, generally speaking, whenever the assumptions of a quasi-linear thin shell analysis are justified, supposing that the torus opening ratio a is not large. A first order improved analysis, developed in Ref. 7 for the membrane case, and its relation to the Liouville transformation used by other authors have been discussed (Chapter IV). A digital computation procedure which is generally suitable for the numerical integration of the quasi-linear shell equations has been developed (Appendix A) and has been used to determine the accuracy of previous tabulations. None of these turned out to be fully reliable.

REFERENCES

1. Jordan, P. F., "On the Stiffness of Thin Pressurized Shells of Revolution," AIAA J. (to be published); NASA CR-60271; Martin Co. RR-61 (November 1964). (An earlier version of this paper is published in AIAA Publ. C-8 (April 1964), pp 200-213.)
2. Jordan, P. F., "Stresses and Deformations of the Thin-Walled Pressurized Torus," J. Aerospace Sci., Vol. 29 (February 1962), pp 213-225.
3. Sanders, J. L., Jr. and Liepins, A. A., "Toroidal Membrane Under Internal Pressure," AIAA J. Vol. 1, No. 9 (September 1963), pp 2105-2110.
4. Clark, R. S., "On the Theory of Thin Elastic Toroidal Shells," J. Math. & Phys., Vol. 29 (1950), pp 146-178.
5. Rossettos, J. N. and Sanders, J. L., Jr., "Toroidal Shells Under Internal Pressure in the Transition Range," AIAA Preprint 65-145. Also Div. of Eng. and Appl. Phys. Harvard U. Tech. Report No. 19 (June 1964).
6. Hetényi, M. and Timms, R. J., "Analysis of Axially Loaded Annular Shells with Applications to Welded Bellows," Transactions ASME, Vol. 82 (2) (1960), pp 741-755.
7. Jordan, P. F. and Shelley, P. E., "Formal Solution of a Nonhomogeneous Differential Equation with a Double Transition Point," J. Math. Phys., Vol. 6, No. 1 (January 1965), pp 118-135, NASA CR-60270.
8. National Bureau of Standards, "Bessel Functions of Fractional Order," Vol. II, Columbia U. Press (1949).
9. Kalnins, A., "Analysis of Shells of Revolution Subjected to Symmetrical and Nonsymmetrical Loads," J. Appl. Mech. (September 1964), pp 467-476.
10. Sepetoski, W. K., Pearson, C. E., Dingwell, I. W. and Adkins, A. W., "A Digital Computer Program for the General Axially Symmetric Thin-Shell Problem." J. Appl. Mech. (December 1962).
11. Dean, W. R., "The Distortion of a Curved Tube Due to Internal Pressure," Philos. Mag., Vol. 28 (1939), pp 452-464.

APPENDIX A

COMPUTER PROGRAM

Consider the general second order equation

$$af + bf' + cf'' = d \tag{A-1}$$

defined in $x_1 \leq x \leq x_2$, and with one boundary condition given at each end. In principle, the numerical solution can be obtained by calculating initially two solutions, one inhomogeneous, one homogeneous, fulfilling the boundary condition at x_1, and combining the two to fulfill the condition at x_2. In practice, both initial solutions will usually diverge exponentially; thus, if x_1 and x_2 are sufficiently far apart, all available accuracy will disappear when the initial solutions are combined.

This "two point boundary value problem" arises frequently, and various methods to circumvent the difficulty have been used, e.g., Refs. 2, 5, 9 and 10. The method of Refs. 5 and 10 is a Gaussian elimination scheme which is based on a finite difference presentation of the given differential equation. By going through the integration interval twice, first in one direction, creating a set of auxiliary quantities, and then in the other direction, calculating the solution f, the use of the homogeneous solution is avoided. This method, which has found wide acceptance in the last few years, is now usually called Potters' method.

It should be possible, and indeed it is, to formulate an analytical equivalent to Potters' method. As an example, assume that f_1' is one of the given boundary conditions. Set

$$f' = u + vf \tag{A-2}$$

Any solution of (A-2) will also be a solution of (A-1) (as is readily verified) if

$$a + bv + c\,(v' + v^2) = 0 \tag{A-3}$$

$$bu + c\,(u' + uv) = d \tag{A-4}$$

To find f, integrate first (A-3 and A-4), starting from $x = x_1$, with boundary conditions $u_1 = f_1'$; $v_1 = 0$. With u and v thus obtained, calculate f by integrating (A-2), starting from x_2, and with the boundary condition there given.

To illustrate the working of the method, consider

$$f - f'' = A \; ; \qquad x_1 = 0$$

The solution is

$$f = A + f_1' \sinh x + B \cosh x$$

If, in the standard method, both the initial solutions are calculated numerically, starting from x_1 with an arbitrary B, then both will diverge, and will be almost undistinguishable for x large. On the other hand, the auxiliary functions

$$\left.\begin{aligned} u &= f_1' \operatorname{sech} x - A \tanh x \to -A \\ v &= \tanh x \to 1 \end{aligned}\right\} \text{ for } x \to \infty$$

remain finite, and integration of (A-2) presents no difficulty.

If (A-1) is homogeneous ($d \equiv 0$) then $u \equiv 0$ is a possible solution of (A-4), and (A-3) becomes the Riccati equation of (A-1). For this reason, the present analytical equivalent of Potters' method may be called the Riccati method.

While the two methods are equivalent in some senses, the Riccati method is more general and, potentially, is much more efficient. In Potters' method one sets

$$f_{i-1} = a_i + b_i f_i$$

and finds

$$a_i = -\delta u_i + 0(\delta^2) \; ; \quad b_i = 1 - \delta v_i + 0(\delta^2)$$

where δ is the finite step size. In the limit $\delta \to 0$ one has $u_i \to u$; $v_1 \to v$. With $\delta \neq 0$ but very small, one has to carry the 1 in b_i, and this leads to the necessity of carrying useless decimals. *

*The authors of Ref. 10 found that the accuracy of their results decreased when they used a very small step-size δ. This observation led us to look for an analytical equivalent of Potters' method.

The relation between the two methods may be summarized by saying that Potters' method uses the finite difference formulation

$$f_i' \approx \frac{1}{2\delta}(f_{i+1} - f_{i-1})$$

$$f_i'' \approx \frac{1}{\delta^2}(f_{i+1} - 2f_i + f_{i-1})$$

which, while it is simple enough to make the Gaussian elimination process feasible, is also notoriously inefficient. The Riccati formulation, on the other hand, makes it possible to use, in the numerical integration, any one of the sophisticated computer methods that have been developed for this purpose.

The Riccati method can, of course, be formulated for systems of differential equations and for arbitrary boundary conditions. We used it to solve the system

$$-f + C^2 f'' - x g = 0$$

$$g'' + x f = x^n$$

compare Eq (33), with $C = \rho^{-3/4}$. Setting

$$Cf' = Cu_0 + u_1 f + \mu g$$

$$g' = v_0 + v_1 g + C\nu f$$

we had to solve initially the set, corresponding to (A-3 and A-4)

$$Cu_0' + u_1 u_0 + \mu v_0 = 0 \quad ; \quad v_0' + v_0 v_1 + C\nu u_0 = x^n$$

$$Cu_1' + u_1^2 + C^2 \mu\nu = 1 \quad ; \quad v_1' + v_1^2 + \nu\mu = 0$$

$$C\mu' + u_1 \mu + C\mu v_1 = x \quad ; \quad C\nu' + Cv_1 \nu + \nu u_1 = -x$$

with the initial conditions at $x = x_1$

$$u_0 = f' \; ; \; u_1 = 0 \; ; \; \mu = 0$$

$$v_o = g' \; ; \; v_1 = 0 \; ; \; \nu = 0$$

The Bowie integration procedure was selected for our exploratory calculation. As this required knowledge of the midpoint values of the auxiliary functions $u_0, u_1 \ldots$ for the backward run, this run was made with the step-size 2δ.

Computer runs for $\rho = 0$ were also made, but with a modified set of equations. For the forward run we tried $\delta = 1/8, 1/16, 1/32$ . . and found that at least 6-decimal accuracy was obtained with $\delta = 1/64$. We made runs with $x_1 = -5$ and with $x_1 = -10$; the latter value was finally selected because it allowed more accurate starting values to be determined (from asymptotic developments) and because it left enough room for edge effects to die out. The integration was continued through $x = 0$ up to $x_2 = |x_1|$; the accuracy of the result could readily be checked by means of the symmetry conditions.

The time used by the IBM 7094 computer for one complete run (one pair of values ρ, n) was about 1 minute.

APPENDIX B

MODEL MANUFACTURE AND TEST PROGRAM

Figure 5 is a schematic presentation of the basic model design. The torus shell was made from two identical half shells, each produced, by means of explosive forming, from a preform (lower half of Fig. 5) consisting of a horizontal flat washer and two conical parts welded from flat sheet material. The center part of each half-shell was a cup that had been made by marforming. One such preform is shown in Fig. B-1, set into the die and ready to be formed explosively.

The preforms were made from 2219-0 bare aluminum. The increase in wall thickness toward the center (Fig. 5) was dictated by an analysis of the stresses to be expected in the welds. All welds, except the weld that tied the two half-shells together at the outer circumference, were heat treated and aged to a nominal ultimate strength of 50,000 psi; the nominal strength of the last weld was 30,000 psi. The completed shell was proof tested to an internal pressure $p = 60$ psi. At this pressure, the safety factor of all welds with respect to the critical stress (N_ϕ, see Fig. 10a)* was above 3 (a few repairs of cracks in welds that had developed during heat-treatment reduced the nominal safety factor to 2 locally).

Where feasible, automatic welding was used on the half-shells. In all cases, careful alignment of parts to be welded was required but not easy to achieve. An elaborate rotating weld fixture with holding clamps was built for this purpose.

The explosive forming, into a die made of kirksite, the forming part of which had been machined on a lathe, was done in several steps. First, by means of one or two explosions, the preform was shaped close to but not touching the wall of the die. The preform was then heat-treated. The resulting

*It can be read from Figs. 10a and 10b that at the crown N_θ due to axial load, applied at $p = 30$ psi, reached about the same magnitude as N_ϕ at 60 psi. There is, however, no weld close to the crown.

Fig. B-1. Half Torus-Shell Preform in Explosive Forming Die

distortion was eliminated, and the final shape was achieved, by means of a final (sizing) explosive shot. After this, the half-shell was subjected to aging.

Before, between and after each operation, all welds were carefully inspected with the dye penetrant technique and were repaired as necessary. Some X-ray inspection of welds was done, but only with trial welds, not with the actual model.

The manufacturing operation that was most critical for the accuracy of the final model was not the explosive forming but the joining together of the two half-shells. Figure B-2 shows details. The required strength in the center (a) was achieved not by a weld (the purpose of the weld here is to contain the internal pressure) but by a prestressed locking bolt with two heavy washer plates. Critical were both the machining of the outer edges of the half-shells in preparation for making the outer weld (b), and the welding operation itself.

Before the two half-shells are welded together, each of them is a rather flimsy structure and is easily deformed. To cut the outer edges requires that the half-shell be held rigidly in its correct shape. The original intention had been to achieve this by means of a male plaster casting, made from the half-shell sitting in the forming die. The cast did not, however, provide proper stability, and a special fixture had to be built.

Not only was the circumferential accuracy of the edge critical but so also was the height of the cut. The latter had to be determined by predicting the shrinkage that would occur during the final welding operation. For this purpose, a number of trial welds were made. It was found that the shrinkage varied considerably, between 0.01 and 0.03 in. Presumably, similar variations occurred circumferentially on the production weld, in spite of precautions taken, and contributed to local shifts of the crown from ideal that were found on the completed shell.

Before the final weld was made, back-up rings were spotwelded to the edges (Fig. B-2) (b), to aid in the alignment of the edges and to act as heat sinks. The perimeter was tack welded at 1-1/2 inch increments before the actual welding was done.

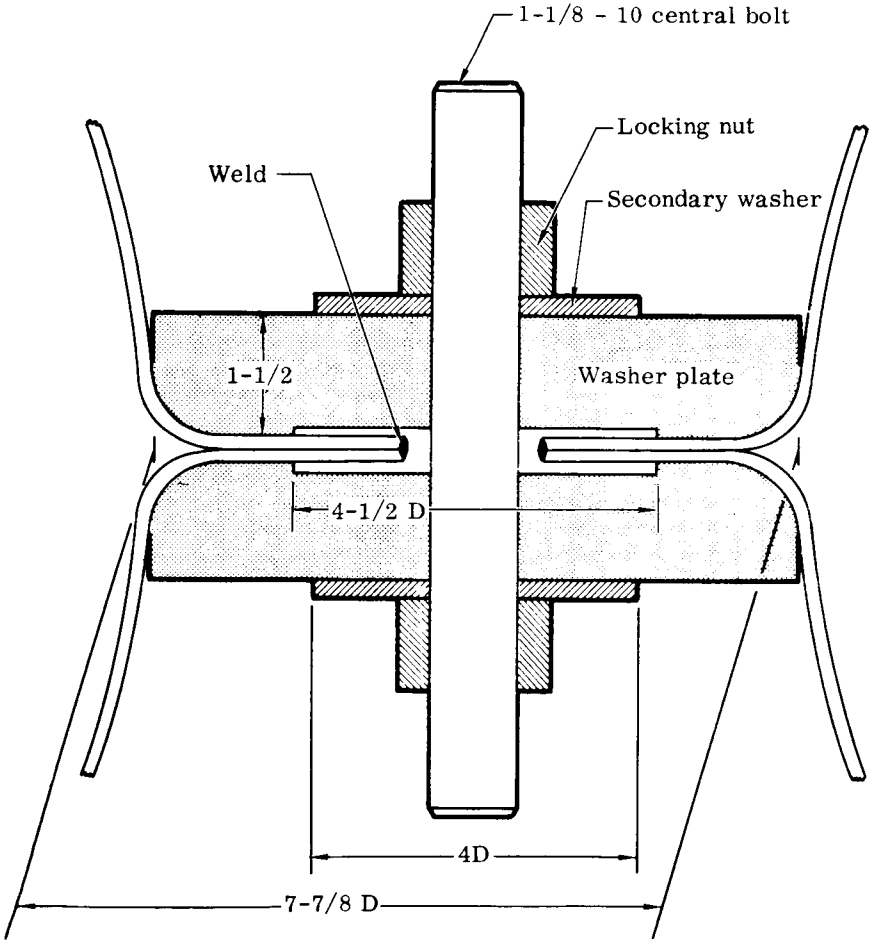

(a) Central Locking Assembly

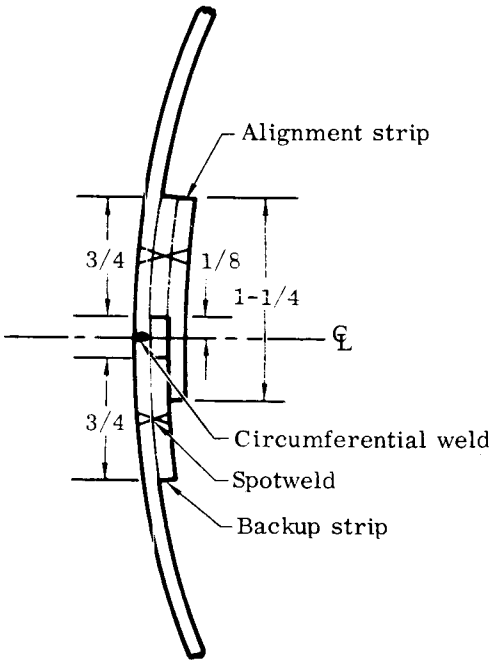

(b) Circumferential Weld

Fig. B-2. Details of Joining Half Shells

The model was completed by inserting the central locking bolt and prestressing it beyond the maximum central expanding load that was to occur during the test program (about 22,000 lb at 30 psi).

The model instrumentation consisted of strain gages, deflection gages and a crown shift meter. Two element strain gage rosettes were bonded along the left upper meridian of Figs. 5, B-3 and B-4 at the following positions:

$\phi_0 =$ -55° ; -37° ; -25° ; -17° ; -12° ; -8° ; -4°
55° ; 37° ; 25° ; 16° ; 10° ; 5° ; 0°

At the underlined positions, back to back rosettes were affixed, one to the inside, one to the outside of the shell, in the two principal directions. At the positions not underlined, and also at the three additional crown positions (Fig. 5) only inside gages were affixed (to make more detailed testing possible later). These inside gages were read during the tests but the readings were not systematically evaluated.

The deflection gages were mechanical dial gages; Figs. 5, B-3 and B-4. The two pairs of gages at the outer right and left and also the central gage read to 10^{-4} inch. Gages reading to 10^{-3} inch were positioned along the strain gage meridian at

$\phi_0 =$ -38°; -18°; -9°; 0° ; 11° ; 26°.

The crown shift meter (Figs. 5 and B-4) was simply a pointer, fixed to an 1/2-inch block that was bonded to the shell at its crown. By reading with a transit the sideways motion of a point near the top and a point near the bottom of this pointer, the angular motion of the pointer was determined.

The overall test arrangement is shown in Fig. B-3. The model was fixed to a support structure, a heavy cylinder with cutouts, by means of 100 T-shaped support lugs (Fig. B-4). To these lugs the model was bonded at its outer circumference, with 1/8-inch thick rubber buffers between lugs and model.

The axial load was applied hydraulically through the central bolt.

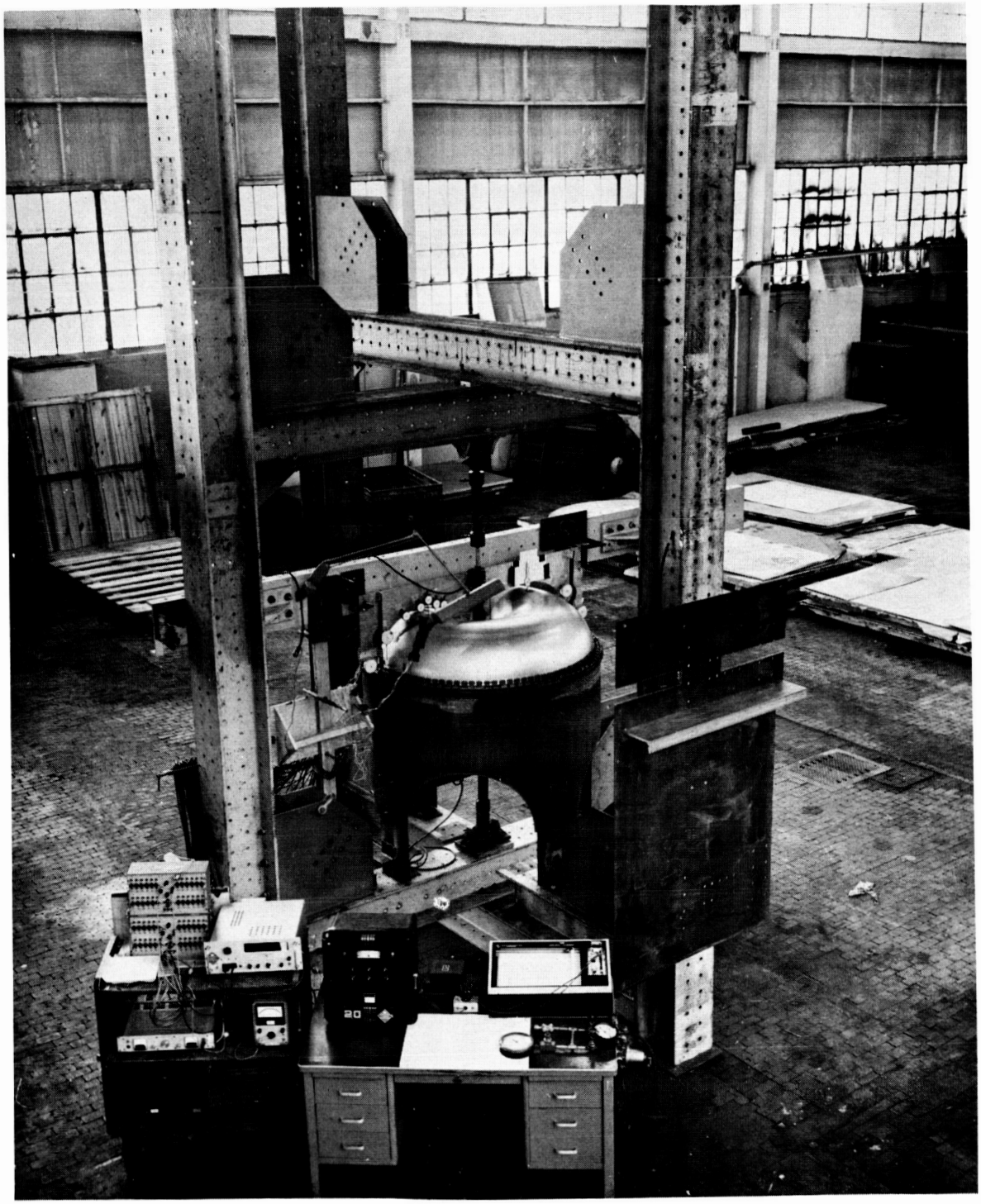

Fig. B-3. Test Setup, Survey

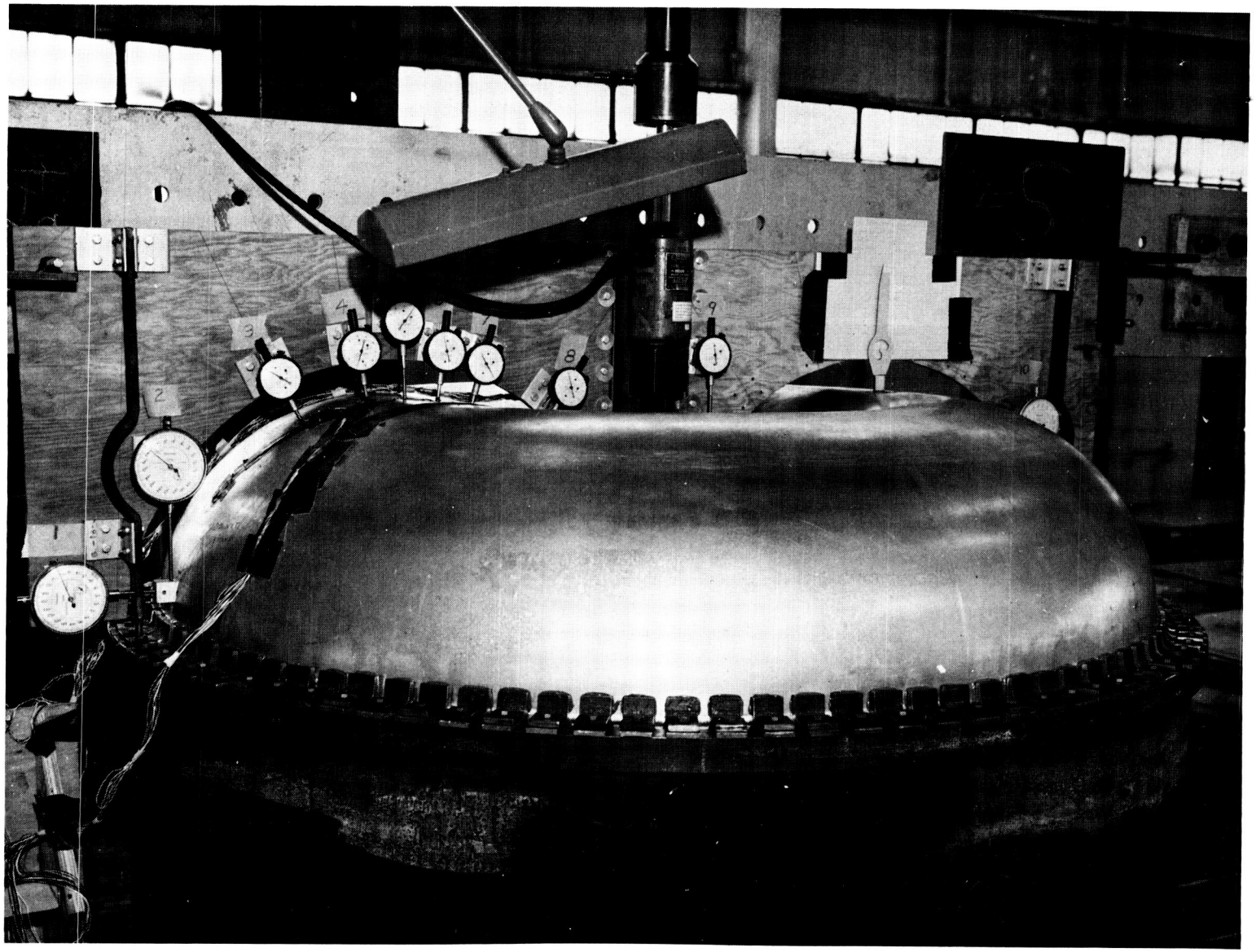

Fig. B-4. Instrumentation Details

The deflection gages were fixed to a vertical plywood plate (Fig. B-4), which rested on the supporting cylinder with knife edges and straddled the model.

The electronic indicating equipment, for internal pressure p, axial load P and strains, is visible in the front of Fig. B-3.

Test pressures were

$$p = 0;\ 3.1;\ 6.2;\ 10;\ 15;\ 20;\ 25;\ 30 \text{ psi}$$

Axial loads were applied both upward and downward, to correspond to a nominal central deflection

$$\Delta = 0;\ 1/16 \text{ inch};\ 1/8 \text{ inch}$$

in an exploratory test series, and

$$\Delta = 0;\ 1/8 \text{ inch};\ 1/4 \text{ inch}$$

in the final test series. The corresponding axial loads can be read from Fig. 6; the load-deflection ratio was constant within the experimental accuracy (this implies, that no indication of approaching shell buckling was found).

A few test observations follow which are not covered in Chapter III of the report. Readings from the two vertical deflection gages at the outer circumference showed that the model support (the T-shaped lugs) did not give measurably under load. The horizontal deflection gages indicated a growth of the overall diameter by 0.005 inch due to p = 30 psi, a growth by an additional 0.002 inch under maximum download (upper shell), and a corresponding reduction under upload. The central deflection gage indicated an upward motion (of the upper central washer plate) due to pressure alone, and about linear with pressure, amounting to 0.021 inch for p = 30 psi. As the central locking bolt was prestressed, this motion could not have been due to a local separation of the two washer plates. The only explanation that remains seems to be that an asymmetry of the model was being corrected by the pressure.

APPENDIX C

COMMENTARY ON A PAPER BY A. KALNINS*

The fact that pressurization of a circular torus shell leads to bending moments near the two crowns of the torus was discovered by W. R. Dean[11]. Dean, and a number of other authors since, proposed to apply linear shell theory to this problem. A. Kalnins seems to be the first to follow this through. His numerical results, obtained by means of modern computer methods, are indeed a very welcome addition to our knowledge.

Kalnins' results do not, however, represent the actual behavior of a pressurized torus shell with a small thickness ratio h/b. This is readily seen. We assume, as does Kalnins, that, as h/b is varied, the internal pressure p is varied simultaneously such that the reference strain pb/Eh remains constant. Kalnins' results imply that the maximum bending stress $\sigma_{\phi b}$ would then be proportional to $(h/b)^{1/3}$, which in turn would imply a curvature change $(h/b)^{-2/3}$. From this result (which is in agreement with analytical predictions) it follows that linear shell theory is not applicable as $h/b \to 0$.

The explanation for this inconsistency lies in the fact that a shell becomes stiffer when it is pressurized; a pressurized shell has a pressure stiffness in addition to its inherent bending stiffness. Linear shell theory disregards the pressure stiffness. On the other hand, a membrane analysis (Ref. 2) which does take the pressure stiffness into account (but neglects the bending stiffness) leads to the result: $\sigma_{\phi b} \sim h/b$, that is, κ_{ϕ} = constant (i.e., the deformed shape is independent of h/b). In this "quasi-linear" analysis, no difficulty arises as $h/b \to 0$.

On the actual shell, pressure stiffness and bending stiffness interact. A complete analysis has to take both stiffnesses into account. Such an analysis

*This discussion of Ref. 9 has been submitted to the Editors of the Journal of Applied Mechanics. It is reproduced here as an illustration of an aspect of the torus problem that has sometimes led to conceptual difficulties.

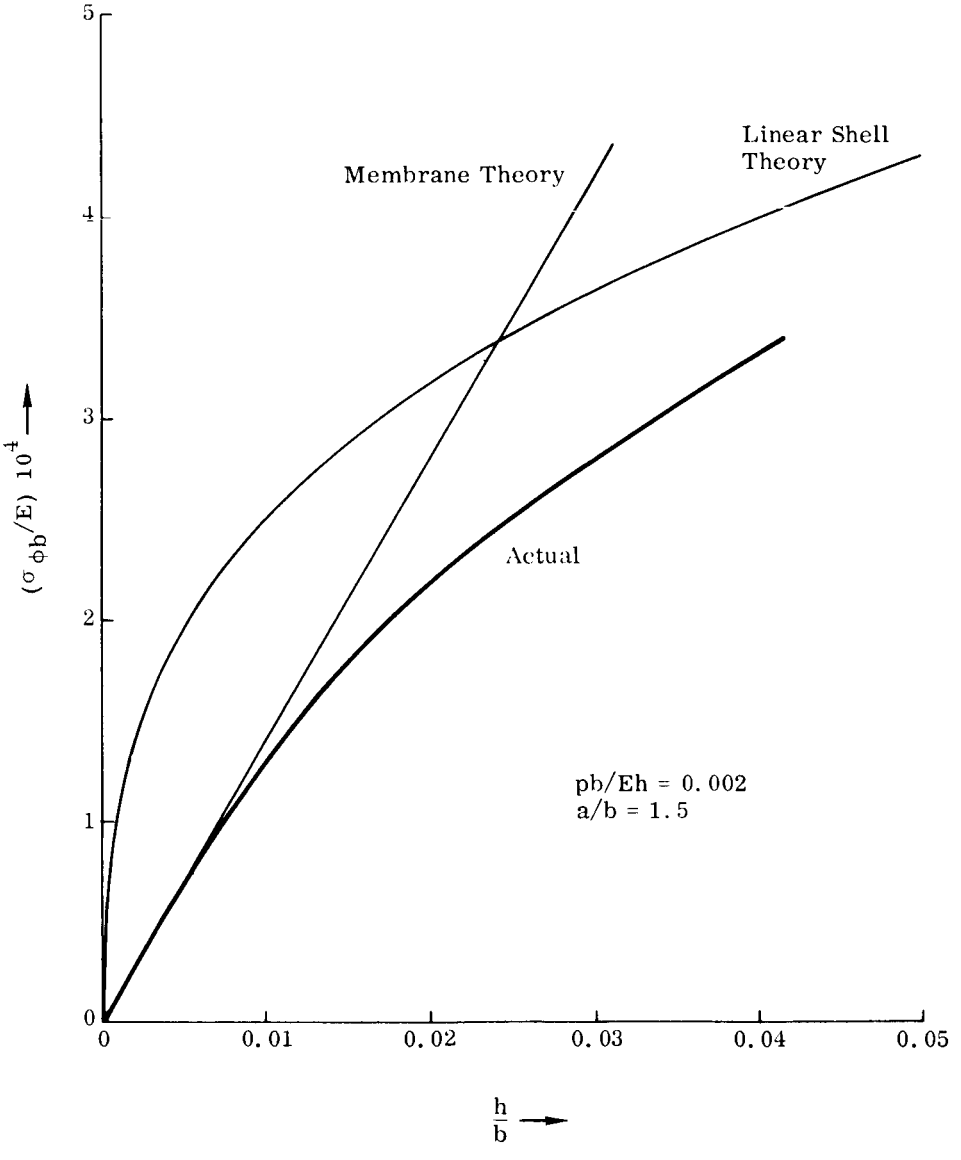

Fig. C-1. Maximum Meridional Bending Stress Due to Pressurization

has been made (Ref. 1) to determine the overall stiffness S of pressurized torus shells with respect to axial loads. It was found: if h/b is finite but small, then the increase of S that arises from the bending stiffness is (about) cancelled by a decrease of the effect of the pressure stiffness on S. As a consequence, the result of membrane theory (Ref. 2) remains valid up to larger values of h/b than might have been expected.

Figure C-1 concerns the case of zero axial load to which Kalnins' calculations refer. The curve "linear shell theory" describes Kalnins' results. The scope for "membrane theory" is taken from Ref. 2. The curve "actual" takes both stiffnesses into account. At the thickness ratio h/b = 0.005 that Kalnins discusses, the linear shell theory result is too large by a factor ≈ 2.7, and the membrane theory result is correct for all practical purposes.